A retrospective and prospective examination of the 1960s U.S. Northeast Drought

Zeyu Xue[1]and Paul Ullrich[1]

[1]Atmospheric Science Graduate Group, University of California, Davis, Davis, California

Key Points:

- Returned 1960s droughts are simulated under warming climate in the early, middle and late century.
- A significant wetting trend emerges; however, it helps little to mitigate the extreme dry months.
- Significant snowpack loss and surface runoff decrease are anticipated for future droughts.

Corresponding author: Zeyu Xue, zyxue@ucdavis.edu

Abstract

As the most severe drought over the Northeastern United States (NEUS) in the past century, the 1960s drought had pronounced socioeconomic and natural impacts. Although it was followed by a persisting wet period, the conditions leading to the 1960s extreme drought could return in the future, along with its challenges to water management. To project the characteristics and potential consequences of such a future drought, pseudo-global warming simulations using the Weather Research and Forecasting Model are performed to simulate the dynamical conditions of the historical 1960s drought, but with modified thermodynamic conditions under the RCP8.5 scenario in the early (2021-2027), middle (2041-2047) and late (2091-2097) 21st century. Our analysis focuses on essential hydroclimatic variables including temperature, precipitation, evapotranspiration, soil moisture, snowpack and surface runoff. In contrast to the historical 1960s drought, similar dynamical conditions will generally produce more precipitation, increased soil moisture and evapotranspiration, and reduced snowpack. However, we also find that although wet months get much wetter, dry months may become drier, meaning that wetting trends are most significant in wet months but are essentially negligible for extremely dry months with negative monthly mean net precipitation. For these months, the trend towards wetting conditions provides little relief from the effects of extreme dry months. These conditions may even aggravate water shortages due to an increasingly rapid transition from wet to dry conditions. Other challenges emerge for residents and stakeholders in this region, including more extreme hot days, record-low snow pack, frozen ground degradation and subsequent decreases in surface runoff.

Plain Language Summary

The 1960s Northeastern United States (NEUS) drought was an abnormally long period of subnormal precipitation with subsequent impacts on water supply, partly countered by its cold temperatures. Under a changing climate, risks persist for returned conditions that drove this historically extreme drought. To project the potential impacts of a reoccurred 1960s drought, this study employs a climate modeling methodology known as pseudo-global warming. This approach aims at representing historical weather events under a warming climate. Results show that under similar dynamical conditions, the NEUS will overall be much wetter with more net precipitation and soil moisture. But these wet conditions do not manifest in all months; wetting trends are only apparent in wet and moderate months. For extreme dry months with historically negative net precipitation, net precipitation is largely unchanged and may even decrease slightly. Future precipitation variability increases and drought tends to initiate faster. Additional challenges arise with more extreme hot days, more severe extreme precipitation, less snowpack, frozen ground degradation and subsequent surface runoff decrease. This research provides extensive projections of hydrometerological conditions under a warming climate that is valuable to water managers, policymakers and stakeholders to ensure they are informed of hydrometerological risks brought by changing climate.

1 Introduction

Both historical observations and climate predictions indicate that climate change is likely to increase the intensity and frequency of extreme weather events such as droughts, floods, wildfires and heatwaves (Kharin et al., 2007; Hayhoe et al., 2007; Pfahl et al., 2017). Among these, droughts are one of the costliest natural disasters, with the most severe droughts having economic impacts greater than $10 billion dollars (Andreadis & Lettenmaier, 2006). However, significant uncertainties persist regarding droughts' frequency and magnitude in a warming climate (Strzepek et al., 2010). Consequently there's an increasing and unmet need for understanding how such extreme droughts respond to climate change.

The Northeastern United States (NEUS) is the most economically developed and populated region in the US, accounting for about 20% of US GDP and population but only 5% of its land area (Hobbs, 2008; of Economic Analysis, 2016). Here, extreme weather events – primarily floods, droughts and snowstorms – result in disproportionate socioeconomic damage. One of the most well known examples of extreme weather in this region was the 1962-66 drought, which had pronounced implications for agriculture and water management practices (Namias, 1966; Barksdale, 1968; Janes & Brumbach, 1965). Although the direct economic damage was not extensive (DeGaetano, 1999), this event has since framed water resource planning in the NEUS. Consequently, a return of the water stresses from this period would have enormous implications. To this end, it important to understand how would such an extreme drought's characters change under future climatological conditions? Notably, the unprecedented 1960s drought was followed by a long wet period that continued through today (Seager et al., 2012). Both historical observations and climate models show continued increase in precipitation over NEUS (Frumhoff et al., 2007); however, this should not imply that droughts here are things of the past. In fact, there is evidence that the risk of potentially even more severe droughts remains (Frumhoff et al., 2007; Burns et al., 2007; Hayhoe et al., 2007). Advances in climate models have made it possible to improve our confidence in these projections, and so it is timely to revisit the nature of drought in this region.

Pseudo-global warming (PGW) is a demonstrably effective method for simulating the effects of global warming. This method not only reduces large-scale model biases and ensures that dynamical conditions are consistent with a historical analogue, but also allows us to directly estimate differences between current and future climatological conditions (Ullrich et al., 2018; Kimura et al., 2007). Using PGW, global climate model (GCM) projections are used to modify the meteorological boundary conditions of the historical 1961-1967 period to reflect the impact of climate change on dry and moderate periods, and speculate on the characteristics of such an extreme drought at the beginning-of-century (2021-2027), mid-century (2041-2047) and end-of-century (2091-2097). This study thus focuses on how the dynamical conditions of this period would manifest in a warming climate.

This paper focuses on trends in hydroclimatic variables and the consequences for society and agriculture. Perhaps the most obvious trend being that there will be significant warming, which is observed to be particularly strong over the wintertime at higher latitudes. This causes a decrease in the number of freezing days, early spring snowpack melt and areas of seasonally frozen ground essentially disappearing by the end-of-century. Further, this warming drives a surge in the number of extreme hot days (those with regional mean heat index larger than 41°C). Even with subsequent increases in evapotranspiration, net precipitation increases over most of the NEUS. Using 24-month long-term standardized precipitation index (SPI24) of net precipitation we project mean meteorological conditions of these future drought analogues to be nearly normal, wet and extremely wet at the beginning, middle and end-of-century. However, the short-term SPI (SPI1) of net precipitation indicates this general wetting trend is primarily manifest during moderate months, and so net precipitation variability increases and is responsible for exacerbating the discrepancy between dry and moderate periods. By end-of-century, an extreme drought could potentially develop in only one month from extremely wet conditions.

Other risks also emerge that threaten water resources in this region. For instance, unprecedented extreme precipitation events will emerge during moderate periods. The 99th percentile of precipitation will increase by more than 50% by the end-of-century compared with analogous years in the 1960s. Widespread flood events are expected to become more frequent, and are likely to impact aging infrastructure. Further, early melt of snowpack will lead to less runoff recharge in the early spring. And degradation of frozen ground will lead to more infiltration of water from surface runoff to soil. In conjunction,

by end-of-century these factors will reduce March surface runoff to below half of historical levels, with impacts for the growing season. These changes have likely consequences for both ecosystems and agriculture in the region.

2 The record-setting 1960s drought

The 1960s drought, which occurred from late 1962 to 1966, has been deemed as the most severe drought in the Northeastern US over last century. Its prominence in the region's water resource planning emphasizes that drought is not only limited to commonly dry regions (Barksdale, 1968; Janes & Brumbach, 1965; Seager et al., 2012; Cook & Jacoby, 1977; Lyon et al., 2005). The drought affected millions of people, and covered an area from New England to Virginia and from the Atlantic Coast to Ohio (Barksdale, 1968). As seen in Figure 1, meteorological dryness was the primary driver of the drought, as temperatures were anomalously low over this period (Namias, 1966). These low temperatures spared the region from potentially more severe impacts (Namias, 1966; Janes & Brumbach, 1965). In the New England Region, negative Palmer Drought Severity Index (PDSI) values, associated with drought conditions, began in 1962 and ended at 1966; however, 1962's annual average PDSI was nearly 0 as the drought's effects only manifested in the latter half of the year. Therefore, in this paper, we refer to the years 1963-1966 as "dry" years and 1961, 1962 and 1967 as "moderate" years. This distinction is important as we will contrast future impacts for dry and moderate periods. The most negative PDSI and lowest soil moisture level of the climatological record occurred in 1965, exemplifying the intensity of the drought and the importance of 1965 as the year with the most pronounced impacts. Therefore, our study uses 1965 as the exemplar dry year and 1961, a year with the largest positive precipitation anomaly of the 1960s, as the exemplar moderate year. Notably, the 1960s drought was at its most severe in the spring, and was driven by precipitation suppression from a low pressure anomaly over the North Atlantic Ocean and a descending, northerly flow over the NEUS (Namias, 1966; Seager et al., 2012).

At the beginning of 1962, there was little indication that the NE was descending into a drought state. Precipitation in the early spring of this year was nominal, but after the 6 months of below-average precipitation that followed, a water shortage gradually began to emerge that depleted the soil being used for irrigation (Barksdale, 1968). By late 1962, most observations of runoff and groundwater were below normal levels, and pronounced impacts to agricultural productivity were being felt in states like New York (Barksdale et al., 1966).

Dryness persisted beyond 1962, and although heavy precipitation occurred in late 1963 and early/late 1964, outside of the growing season this did little to prevent the spread of drought (Barksdale, 1968). Consequently, the growing season of 1964 was recorded as the driest of the last century (Janes & Brumbach, 1965). The drought intensified further in 1965 and spread over a wider swath of the northeast. Besides limiting water use, the drought also had an impact on water quality (Barksdale, 1968), as previously unused and polluted water sources began being used to counter water shortages. Rivers' pollutant concentration increased due to insufficient dilution, and sea water intrusion threatened coastal freshwater quality.

Strict rules on water conservation and better management helped greatly in managing the water shortage from 1965 to 1966. Several new regulations were introduced that included prohibitions on washing of automobiles and urban irrigation. At last, the drought ended with abundant precipitation in September 1966 (Barksdale, 1968), with regional mean PDSI rising above zero for the first time in four years.

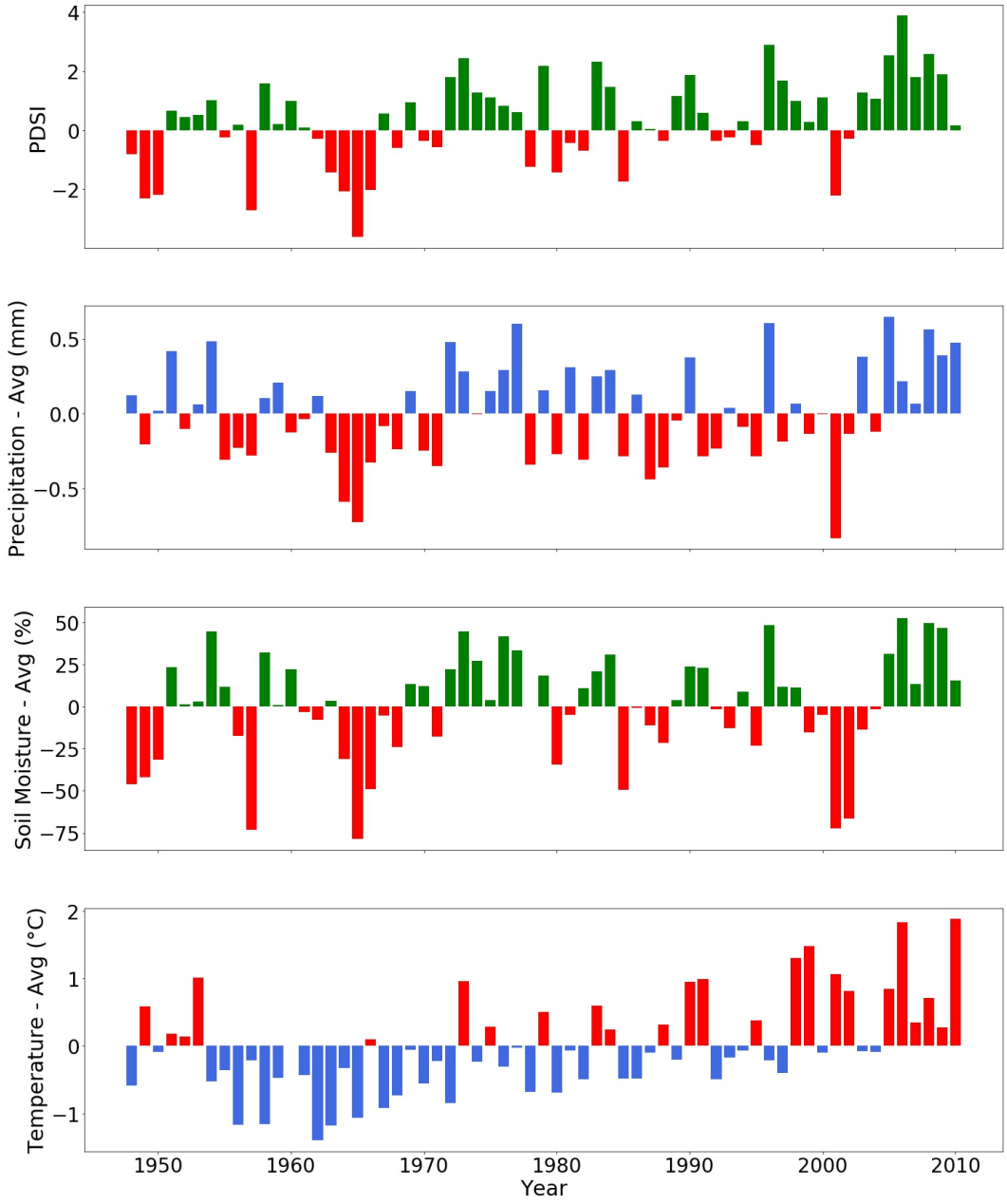

Figure 1. Palmer Drought Severity Index (PDSI) and the anomalies of precipitation, temperature and soil moisture from 1948 to 2010 over the New England Region. PDSI data from NCAR (Dai et al., 2004). Soil moisture data from PSL (Van den Dool et al., 2003). Precipitation and temperature from CERA20C R7 (European Centre for Medium-Range Weather Forecasts, 2016).

3 Uncertainty of a return to drought conditions under climate change

Large uncertainty remains for future trends of drought in the NEUS. Studies generally conclude that although the region is becoming wetter, drought – especially short-term drought – will occur more frequently and intensely under climate change (Frumhoff et al., 2007; Hayhoe et al., 2008; Demaria et al., 2016). Nonetheless, drought is an emergent feature that is affected by changes in thermodynamics (e.g. increases in atmospheric water vapor), hydrology (e.g. precipitation phase, runoff, related land surface variables, and surface-atmosphere fluxes) and dynamical conditions (shifts in the frequency, intensity or duration of meteorological patterns). Overall, both historical observations and model projections indicate an upward trend in average temperature (0.3°C/0.5°F per decade since 1970, with wintertime warming of 0.7°C/1.3°F per decade) and a slight increase in average runoff and evapotranspiration (Hayhoe et al., 2007; Frumhoff et al., 2007; Seager et al., 2012). This has meant more extreme heat days, early melt dates, a lower snowfall-rainfall ratio, and a longer growing season along with more water demand (Frumhoff et al., 2007; Seager et al., 2012; Burns et al., 2007; Hayhoe et al., 2007). Although increased precipitation has meant that drought indices such as SPEI and SPI are shifting towards more positive values, indicative of generally wetter conditions, the spread of these indices is also increasing; consequently, the probability of extreme drought is largely unchanged in both observational data and models (Krakauer et al., 2019).

Water resource planning in the NEUS is highly reliant on a model drought based off of the 1960s drought period. Given subsequent climatic shifts (and foreseeable climatic shifts), there are concerns with the use of a model drought from more than a half century ago (Moser et al., 2008). Consequently, NEUS water management agencies agree that this model drought should be revisited in light of climate change. In the future, earlier snowmelt dates and reduced wintertime snowpack will certainly impact seasonal availability of water (Frumhoff et al., 2007; Burns et al., 2007; Huntington et al., 2004). Future warming will lead to a longer growing season and enhanced evaporation, thus enhancing consumption of available freshwater, particularly in spring and summer (Seager et al., 2012; Frumhoff et al., 2007; Lyon et al., 2005). While the 1960s drought is notable for its severe water shortage in these seasons, its socioeconomic impacts were also tampered by low temperatures. Capturing these factors under climate change motivates the use of a comprehensive model-based study of this period.

4 A simulation of present and future analogues of the 1960s drought

Having motivated the purpose of our study, we now present our methodology and results from our simulations using pseudo-global warming, including temperatures, precipitation, evapotranspiration, snowpack, soil moisture, runoff, and drought indices.

4.1 Methodology

In this study the Weather Research and Forecasting (WRF) Model is used for simulating the regional atmosphere of the NEUS (Skamarock et al., 2008; Powers et al., 2017). WRF is one of the most commonly-employed regional climate modeling systems currently available, incorporating many widely-recognized physical parameterizations. Thousands of research studies have been conducted with WRF worldwide, demonstrating WRF's utility for robust simulation of regional climate. With an appropriate choice of parameterizations, WRF has been shown in past studies to accurately reproduce the hydroclimatology of the NEUS (Ganetis & Colle, 2015). In this study WRF 3.9.1 is used with the parameterization suite given in Table 4.1. The land surface model employed is the Community Land Model 4 (CLM 4) (Oleson et al., 2010), which is the most complicated and expensive of the available options in WRF, but one that shows reasonable performance across a variety of geographies (Ullrich et al., 2018; Jin et al., 2010; Case et al., 2008).

Table 1. Physical parameterizations used in our WRF simulations.

Process	Parameterization
Microphysics	CAM V5.1 two-moment five-class (Neale et al., 2010)
Radiation	RRTMG (Iacono et al., 2008)
Surface layer	Revised MM5 similarity theory (Jiménez et al., 2012)
Land surface model	CLM4 (Oleson et al., 2010)
Planetary boundary layer	UW (Bretherton & Park, 2009)
Cumulus parameterization	ZM (G. J. Zhang & McFarlane, 1995)

4.1.1 Simulation period and domain

Our simulations in this paper cover four time periods: historical (1960-1967), present-day (2020-2027), mid 21^{st} century (2040-2047) and late 21^{st} century (2090-2097). In each simulation the first year serves as the spin-up period to ensure hydrologic and meteorological conditions have stabilized. Two nested domains are used (Figure 2). The outer and inner domains have 105×89 and 187×133 grid points, with resolutions of 18 and 6 km, respectively. Due to the long duration of the simulation, spectral nudging is employed (with the default relaxation timescale) so as to reduce internal model drift. In our simulations the 30-arc second ($\sim$ 1 km) resolution United States Geological Survey-based land use and land cover and topography datasets are interpolated to the model grids as geographical input.

Although most of our analysis focuses on the inner domain (Figure 2), some detailed analyses are conducted within the southern New England subregion (defined as 41N to 43N latitude and 74W to 70W longitude). This location comprises the most populated and developed areas of the NEUS.

4.1.2 Modified forcing from pseudo-global warming

Lateral forcing data for this historical period is from the 6-hourly Coupled ECMWF Re-Analysis system of the 20th-century (CERA-20C) R7 interpolated to 0.5° resolution. CERA-20C is a coupled reanalysis dataset with global coverage from 1901-2010, designed to capture low-frequency climate variability (European Centre for Medium-Range Weather Forecasts, 2016). This dataset is chosen because of its relatively high spatial and temporal resolution, and because its precipitation amounts best match observations of mean precipitation over the NEUS. After comparing the performance across all 10 CERA-20C ensembles, we selected the CERA-20C R7 ensemble as it again provided the highest performance among ensembles. More details on the evaluation protocol are provided in the Supporting Information Text S1.

Anticipated future changes to lateral forcing under climate change are derived from Coupled Model Intercomparison Project phase 6 (CMIP6) projections. In this study we use data from the multi-model mean of four CMIP6 models with demonstrably good performance in the NEUS region (namely, CESM2, MRI-ESM2-0, CNRM-ESM2-1 and GFDL-CM4), as identified by (Srivastava et al., 2020). Following (Ullrich et al., 2018), the spatially averaged monthly mean projections are used to calculate the difference between each of the 2020s, 2040s, and 2090s periods against the 1960s period. Both temperature and relative humidity are assessed in this manner. The resulting temperature differences as a function of month and altitude are depicted in Figure S1. We observe a positive temperature delta throughout the troposphere (up to around 100 hPa altitude), with a local maximum occurring around 350 hPa over the summer, and at the surface over win-

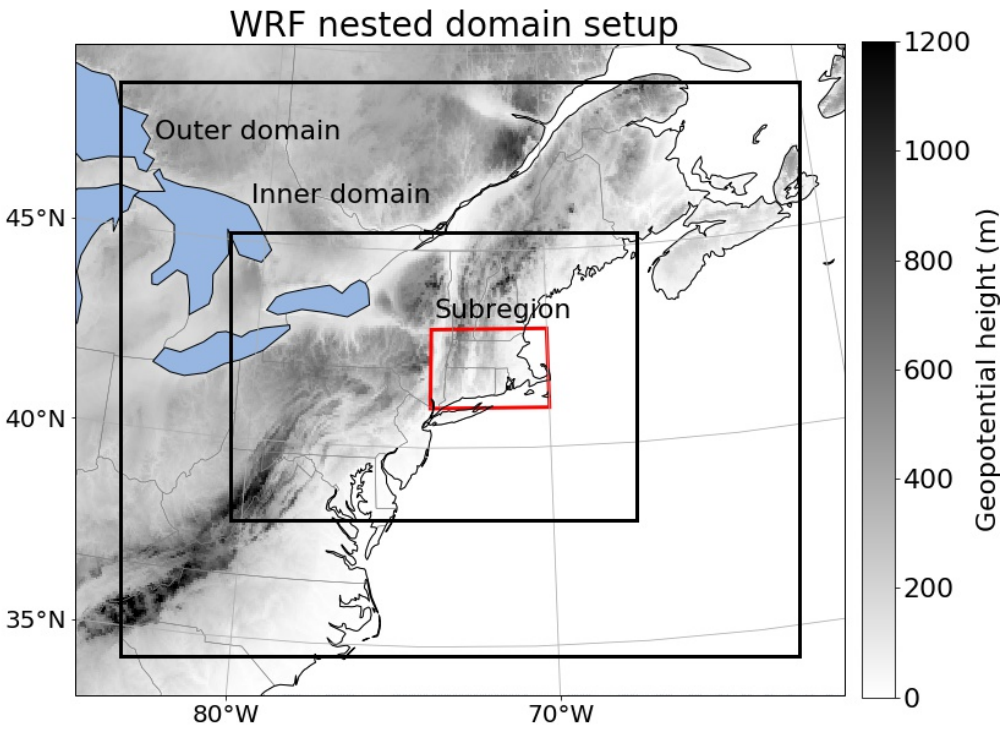

Figure 2. Our WRF domain setup for all simulations in this study. Shading indicates the surface height. Grid spacing in the outer (inner) domain is 18 km (6 km).

ter. There is a negative temperature delta in the stratosphere, as anticipated under climate change. The magnitude of the temperature delta (both positive and negative) clearly increases from the 2020s to the 2040s and the 2090s, although the patterns are consistent. Relative humidity differences are small and so are not shown.

Lateral forcing data for the future simulations are the same as historical, except with the temperature delta (Figure S1) added over the entire domain, on constant pressure surfaces. Based on our observation of essentially negligible changes in relative humidity, relative humidity is held fixed (resulting in enhancement to specific humidity). Sea surface temperatures are analogously modified using the multi-model mean of the selected CMIP6 models to accord with the change to air temperatures. Finally, greenhouse gas concentrations are modified in WRF's radiation parameterization in accordance with the RCP8.5 emission scenario.

4.2 Annual mean temperature and precipitation percentiles

Simulated annual mean temperature and precipitation over our subregion for each year of the drought period is depicted in Figure 3 where historical data comes from CERA20C R7 and simulations are corrected by the regional mean difference between historical data (1961-1967) and WRF 1960s simulation. This plot also gives us a quick glimpse of how the climate of this region is projected to change: Whereas all years of the 1960s were below the 50th percentile of precipitation and most were below the 50th percentile of temperature, each simulated year of the 2040s and 2090s is above the 99.9th percentile of temperature, and all years of the 2090s are well above the 95th percentile of precipitation. This figure clearly highlights the significant regional shift towards a future warmer and wetter climate.

4.3 Temperature

From the CMIP model ensemble, the average warming rate over land from the 1960s period to 2090s period is 0.052°C per year, which is higher than the observed global warming rate over land and ocean since 1981 (0.018°C per year) (Lindsey & Dahlman, 2020). Simulated warming of this magnitude is not unreasonable, as warming is expected to be much stronger over land and at higher latitudes (Hoegh-Guldberg et al., 2018). Figure 4 shows the spatial pattern of 2m temperature from historical and its corresponding change. In general the magnitude of warming intensifies from the 2020s drought to the 2040s and the 2090s droughts, in accordance with expectations from the CMIP6 models under RCP8.5. However, the spatial and seasonal distributions of warming are uneven, with a stronger warming trend in winter (DJF) and at higher latitudes, where historical temperatures are lower; for example, regional mean change over land in 2045 DJF (4.14°C) is 1.52°C larger than 2045 JJA (2.62°C). From Figure 5, a clear correlation between future 2m temperature change and historical mean temperature at each grid point emerges, with enhancement of the change in the winter season and under increased forcing; for example, the correlation over the 2095 winter (-0.62) is much larger than over the 2095 summer (-0.53), the winter of 2045 (-0.50), and the winter of 2025 (-0.43). This trend suggests that cold regions will be warming faster than warm regions, indicative of some homogenization of temperatures over seasons and regions. Thus temperature spatial and temporal variability are reduced, in turn driving earlier snowmelt and intensified evapotranspiration.

Do these trends also hold for moderate periods? Although the lateral temperature deltas of both the dry periods (1963-1966) and moderate periods (1961, 1962 and 1967) are the same, the simulations produce greater regional warming during moderate periods than dry periods (although the difference is small). Further, some differences in spatial distribution of temperature change persist: From Figure 4 (fourth row), we can see that during the moderate wintertime period, the regions with highest temperature change

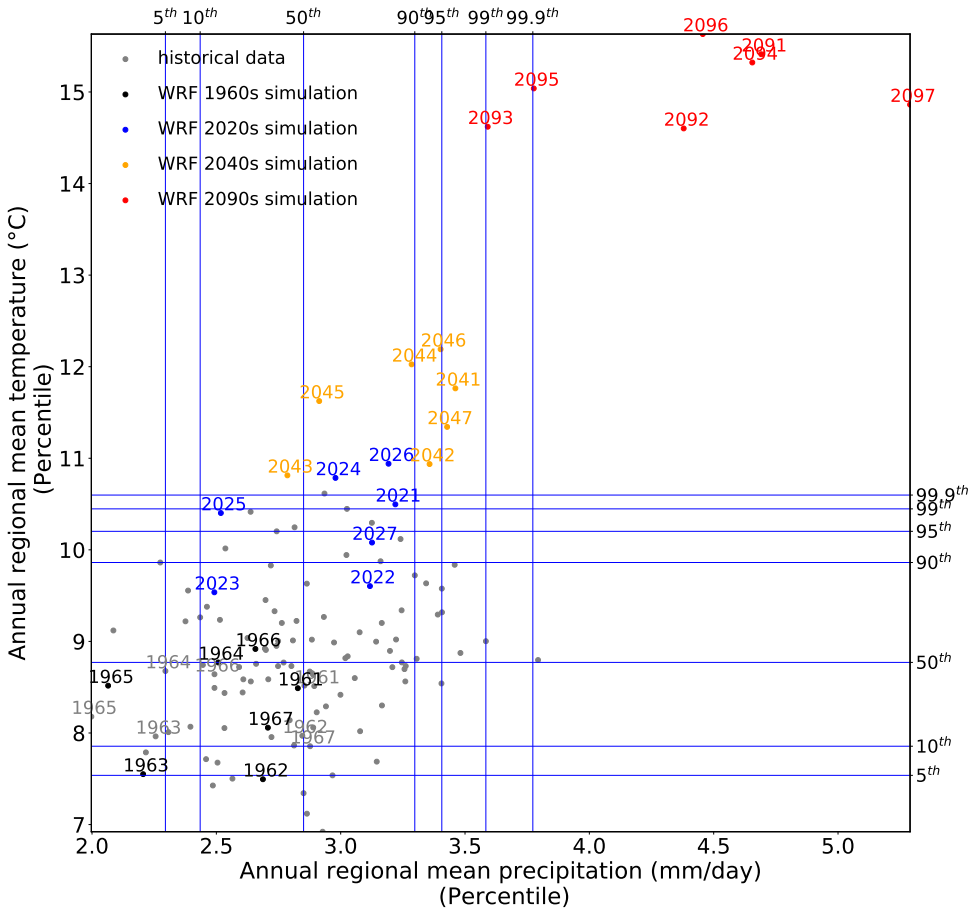

Figure 3. Regional annual mean precipitation and 2 meter temperature within the subregion during historical and future periods, as compared with historical percentiles over the period from 1910 to 2010.

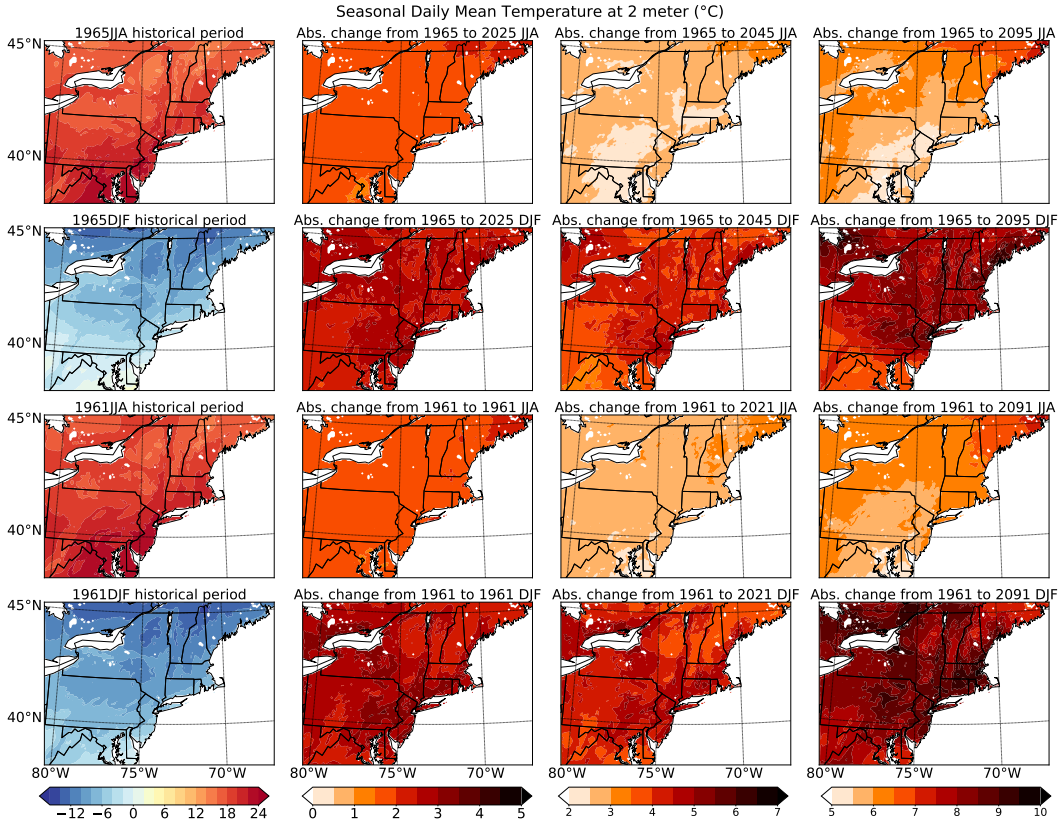

Figure 4. Average daily 2m temperatures (in degrees Celsius) over June-July-August (JJA) and December-January-February (DJF) in 1965 and 1961 (and their future analogues), exemplary of dry and moderate years.

are along the southern extent of New England; however, dry years have the greatest warming along northern extent of the New England (Figure 4, second row). These wintertime spatial differences have consequences for dry years and non-dry years, such as shifts in the number of freezing days and snowmelt (touched on later).

4.3.1 Extreme temperatures

It is well known that shifts in mean temperatures will have a disproportionate influence on the frequency of extreme temperatures. From figure 6, there is a clear increase in the mean annual maximum 2m temperature at all grid points, with more extremely hot days in the future; however, there is essentially no change in the annual variance of temperatures. With that said, both the mean and outliers of annual maximum daily temperature increase more in dry years rather than moderate years, which consequently drives an increase in evaporation and risk of flash drought. Frequency of extreme heat days are assessed using the Heat Index (HI) (Rothfusz & Headquarters, 1990) to better distinguish extremely hot days with potential for significant socioeconomic impact (see Supporting Information Text S2 for the detailed definition of the Heat Index).

As defined by NOAA, values of HI larger than 41°C indicate dangerously hot conditions which may trigger sunstroke, heat cramps and heat exhaustion (NOAA, 2020). Figure 7 shows changes in the number of extreme heat days for each period for the subregion. Compared with historical conditions (noting that this was a relatively cool pe-

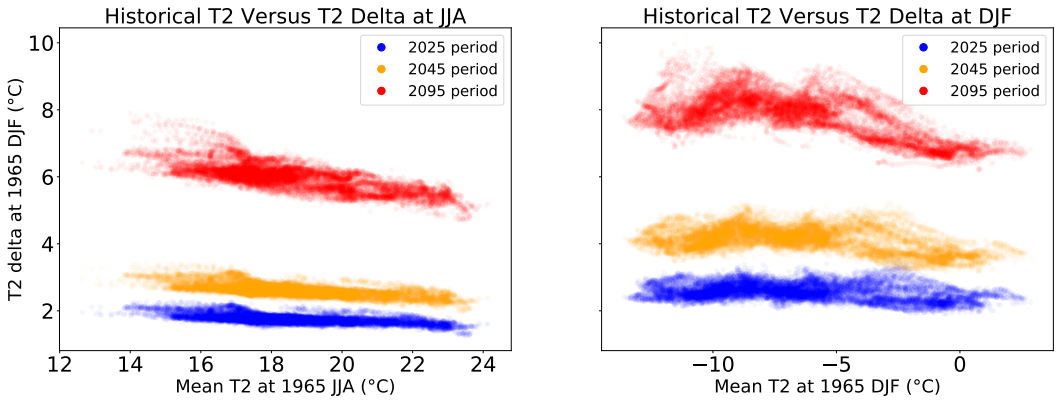

Figure 5. The relationship between historical mean daily 2m temperatures and future 2m temperatures deltas over JJA and DJF in 1965 drought conditions.

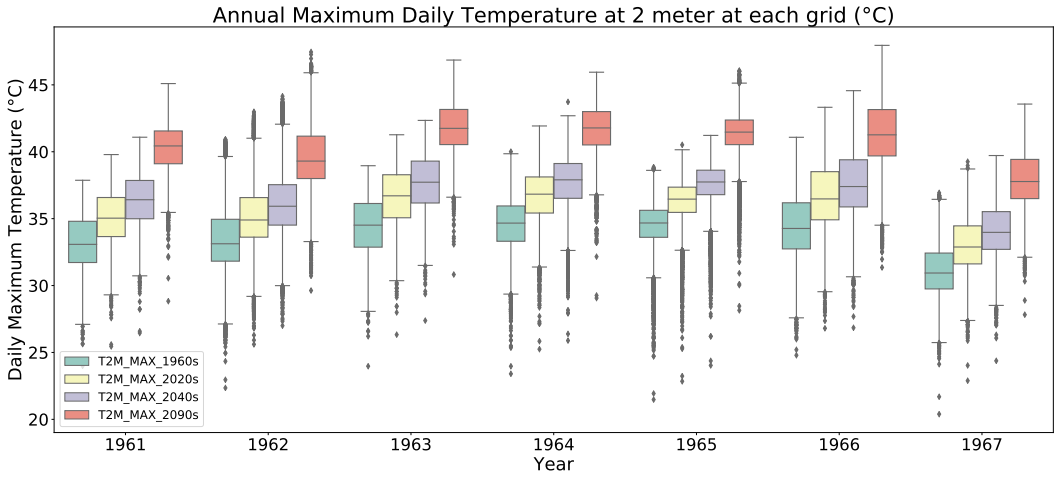

Figure 6. Annual maximum daily 2m temperature (in degrees Celsius) at each grid point.

riod), the number of extreme hot days increases from 6 in 1965 to 27 in 2045 and 56 at 2095. It's clearly the case that extreme heat will be a major public health concern in the NEUS going forward.

The warming climate will also reduce the number of freezing days (days with daily 2m temperature minimum less than 0°C) significantly in both dry year and moderate year (Figure 8). The change in freezing days is highly correlated with change in winter-time T2 (Figure 4). Further, the spatial distributions of the change in freezing day count differs significantly between our exemplar dry year (1965) and moderate year (1961), in accord with their associated temperature deltas and historical number of freezing days. Higher latitudes produce greater decreases of freezing days, where historical freezing days are more common and warming is larger. In these regions, we thus expect degradation of frozen ground (T. Zhang et al., 2003), which we will revisited later.

4.4 Precipitation

Figure 9 depicts seasonal mean daily precipitation over the historical and projected periods. Increasing precipitation is apparent in most regions, especially along the south-eastern coasts during winter and in the southwest during summer. These increases are

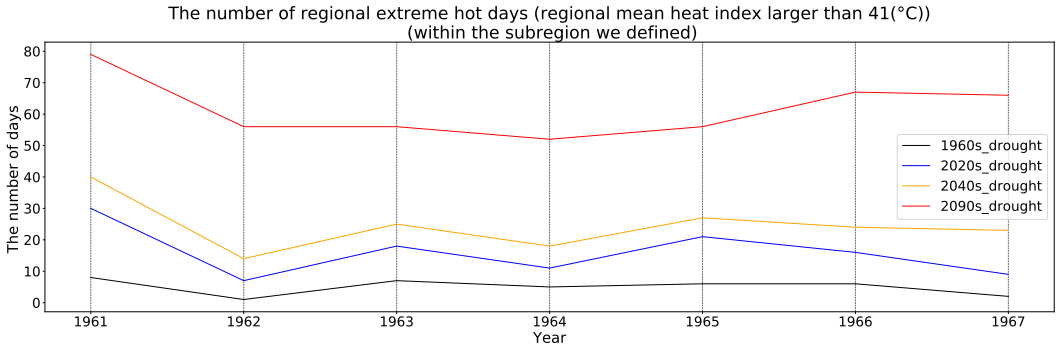

Figure 7. The number of regional mean extreme heat days (regional mean Heat Index larger than 41°C) for the historical period and each future analogue.

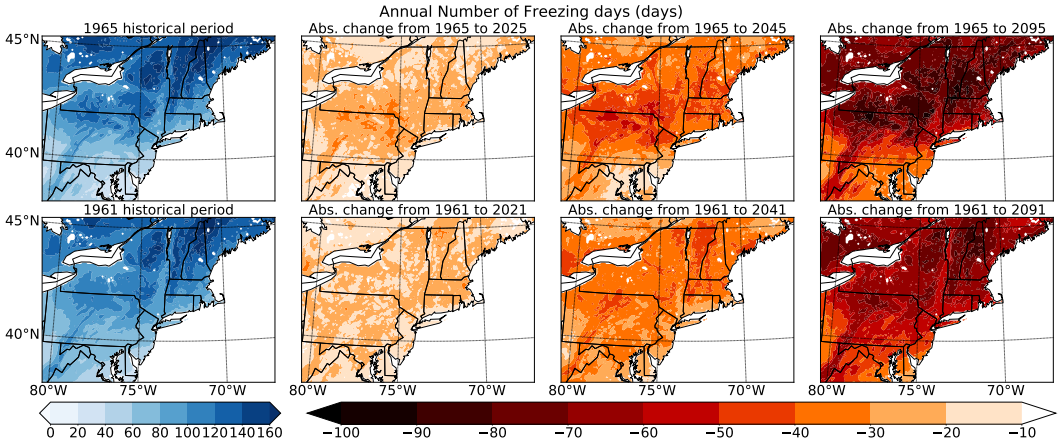

Figure 8. The number of freezing days in 1965 and 1961 (and their future analogues), defined by daily minimum 2m temperature less than 0°C.

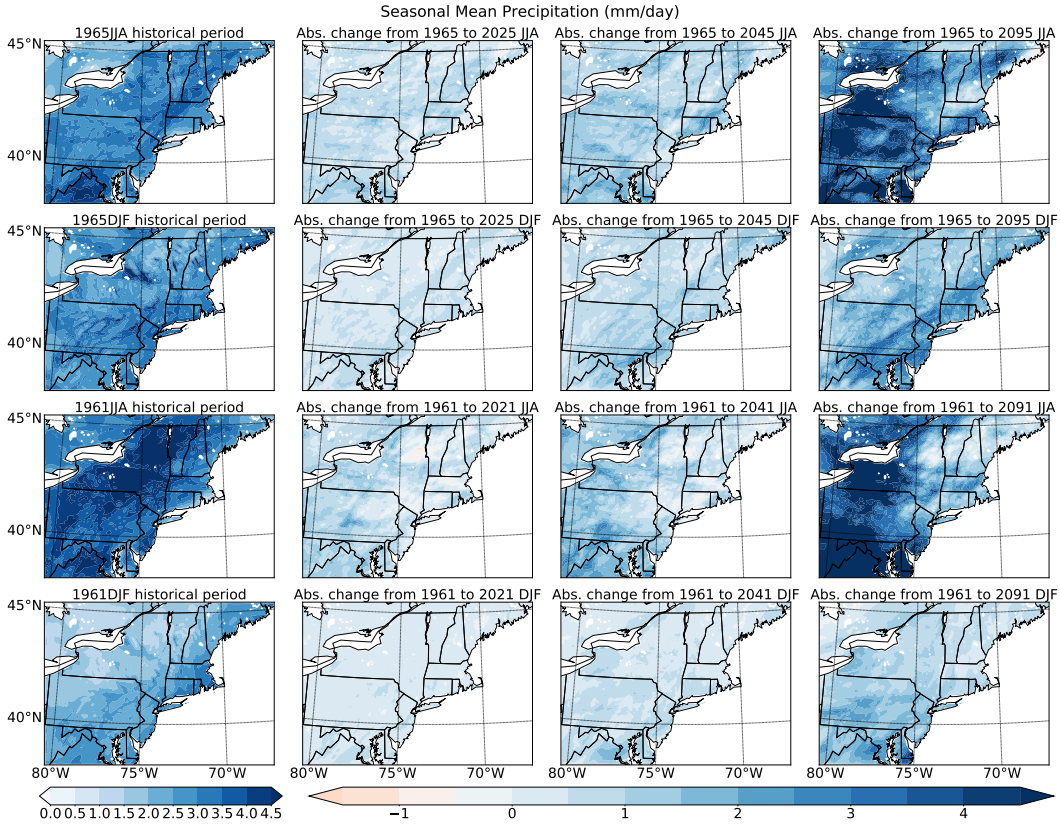

Figure 9. Seasonal mean precipitation distribution and change in the exemplar 1965 dry year and 1961 moderate year (mm/day).

expected because of an intensified hydrological cycle in the warming climate (Huntington et al., 2004; Pfahl et al., 2017). In the literature, the rule-of-thumb of warming climates 'wet becomes wetter' (Donat et al., 2016; Chou & Neelin, 2004; Seager et al., 2010) has been often employed to explain precipitation change over the ocean (Byrne & O'Gorman, 2015); nonetheless, it also applies here (especially in the winter season). In Figure 9 regions with greater precipitation increase coincide with regions of larger historical mean wintertime precipitation, with pattern correlation in 2025 DJF, 2045 DJF and 2095 DJF of 0.51, 0.55 and 0.50, respectively (Figure S6). This result also applies for all other dry and moderate years, with even higher correlations of 0.8 in some cases (e.g. 2043 and 2093 DJF). The applicability of this rule of thumb to the inland NEUS is likely a consequence of a relative abundance of water vapor in the region from the Atlantic Ocean and Gulf of Mexico. What's more, unlike the dry period, the moderate period doesn't experience more precipitation in the northeastern part of the inner domain; however, as we will discuss later, this region experiences a significant soil moisture increase during the moderate period.

Although this study is focused on drought, the dramatic increase in future precipitation deserves some discussion. Extreme precipitation is notorious for its disastrous impacts on society, and has been increasing in frequency across the continental US. This increase is particularly pronounced over the NEUS (Huntington et al., 2004; Hayhoe et al., 2007), where the most intense daily precipitation events (99th percentile daily precipitation) have increased by more than 70% from 1958 to 2012 (Melillo et al., 2014). Our simulations also indicate that more extreme precipitation events will occur here in the future. Figure 10 shows that both absolute and relative precipitation percentiles will

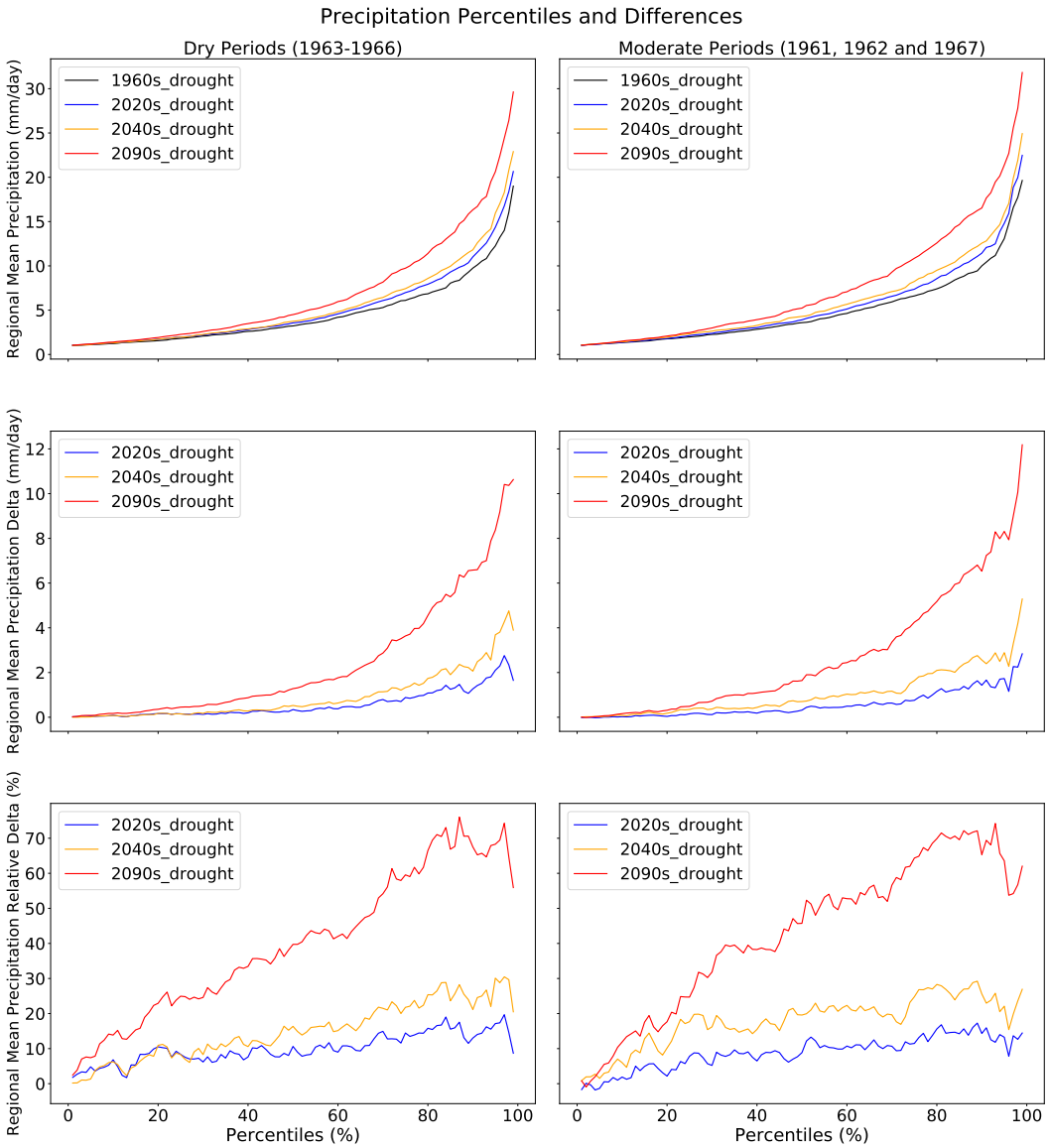

Figure 10. Regional mean precipitation change at different percentiles. Only daily precipitation events larger than 1 mm/day are included.

increase, with greater increases from the 2020s to the 2090s. In particular, the 99th percentile of precipitation will increase more than 50% in both dry and moderate periods in 2090s versus the 1960s. Examining inner domain grid points' annual maximum precipitation (Figure 11), the mean and upper tail of the annual maximum precipitation distribution both increase into the future. We expect unprecedented extreme precipitation (daily precipitation larger than 160 mm/day) may occur (especially in non-dry years) that will challenge the capacity of flood control equipment in NEUS.

4.5 Evapotranspiration

Enhanced evapotranspiration can directly reduce the net input of water from atmosphere to land, decrease runoff and soil moisture, and increase water demands for agriculture and ecosystems. Figure 12) shows that our future analogues exhibit greater sum-

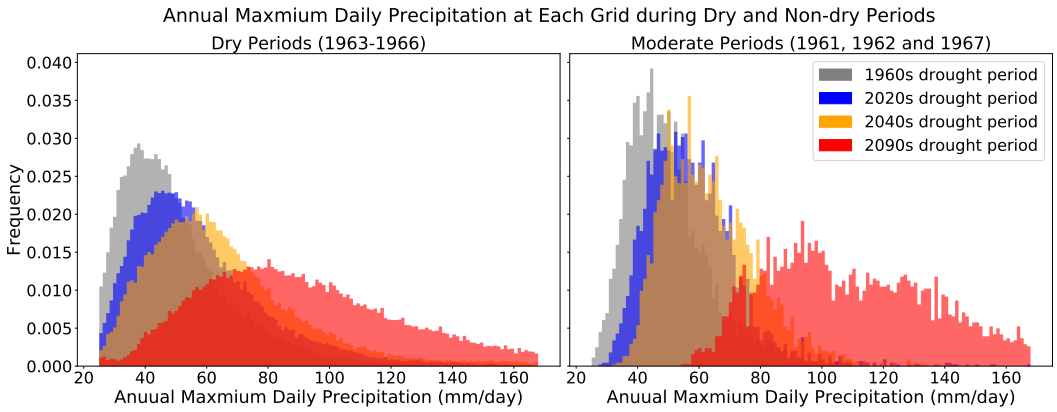

Figure 11. Annual maximum precipitation distribution of all grid points within the inner domain.

mertime evapotranspiration compared to winter, in accord with the spatial and temporal distribution of historical precipitation (Figure 9). Of course, this is unsurprising as evapotranspiration amounts are closely related to water available. Evapotranspiration also increases more toward higher latitudes because of the warming effect, especially in wintertime. These trends hold for all dry and moderate years (Figure 9). Moderate periods producing stronger evapotranspiration intensity are likely caused by more significant warming and more abundant precipitation.

As noted earlier, precipitation increases correlate with historical precipitation. Considering the strong relationship between the evapotranspiration and precipitation change, this inspires the question "how does a net precipitation (precipitation minus evapotranspiration) change emerge?" Figure 13 shows that although evapotranspiration increases, precipitation increases more rapidly, thus producing an overall increase of net precipitation. Consequently, our earlier use of "wet becomes wetter" also applies to net precipitation, especially in winter months where correlations are more than 0.6 (and up to 0.87) between historical net precipitation and its change during both dry and moderate periods. It's further clear that the dry period summertime has much less net precipitation than the moderate period, suggesting that net precipitation is valid for indicating drought conditions. Note that the wet conditions of 1965 DJF was caused by a short-term abundant historical precipitation event.

4.6 Snowpack

Due to its connection to the hydrologic cycle, water supply and ecosystems in the NEUS, an understanding of future snowpack is necessary for water resource planning. Figure 14 shows a clear and rapid decrease in snowpack in this region in DJF and MAM in response to warming. Within the inner domain, seasonal regional mean snow water equivalent (SWE) was 20.56 kg/m^2 in 1965 DJF; however, 2095 DJF only produced 7.16 kg/m^2 of SWE (a 61% decline). This decrease is most pronounced in the spring season (MAM); 2095 MAM exhibits a 94% drop in SWE over 1965 MAM (Figure 15). Lower latitudes are most strongly impacted as here snow is more sensitive to temperature increases. The result is a loss of spring snowmelt contribution to runoff (Figure 14).

Although there is a greater absolute SWE loss over the moderate period, the relative change in the 1961 moderate year (Figure 14) is still much smaller than in the 1965 dry year (Figure 14). Notably, during the 1965 dry period there is practically no historical snow accumulation in spring over the northeastern states of the NEUS (Figure 14),

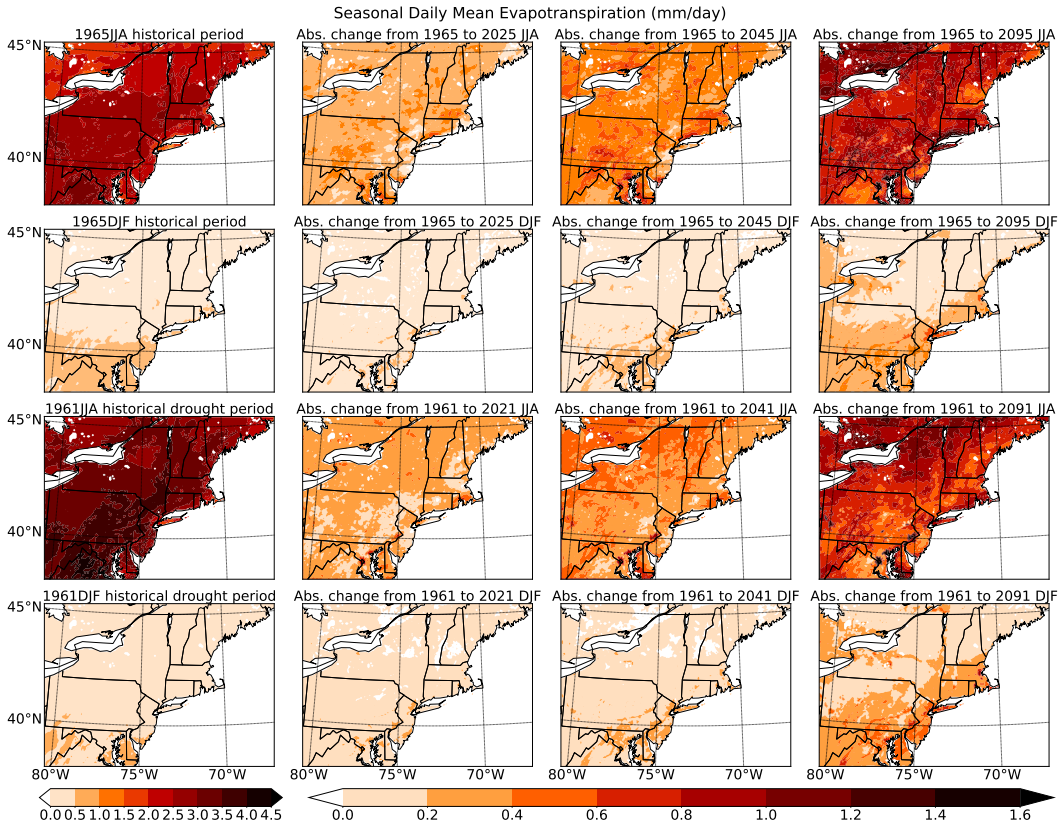

Figure 12. Seasonal mean evapotranspiration (mm/day) over the 1965 dry exemplar and 1961 moderate exemplar,and projected changes in their future analogues for the JJA and DJF seasons.

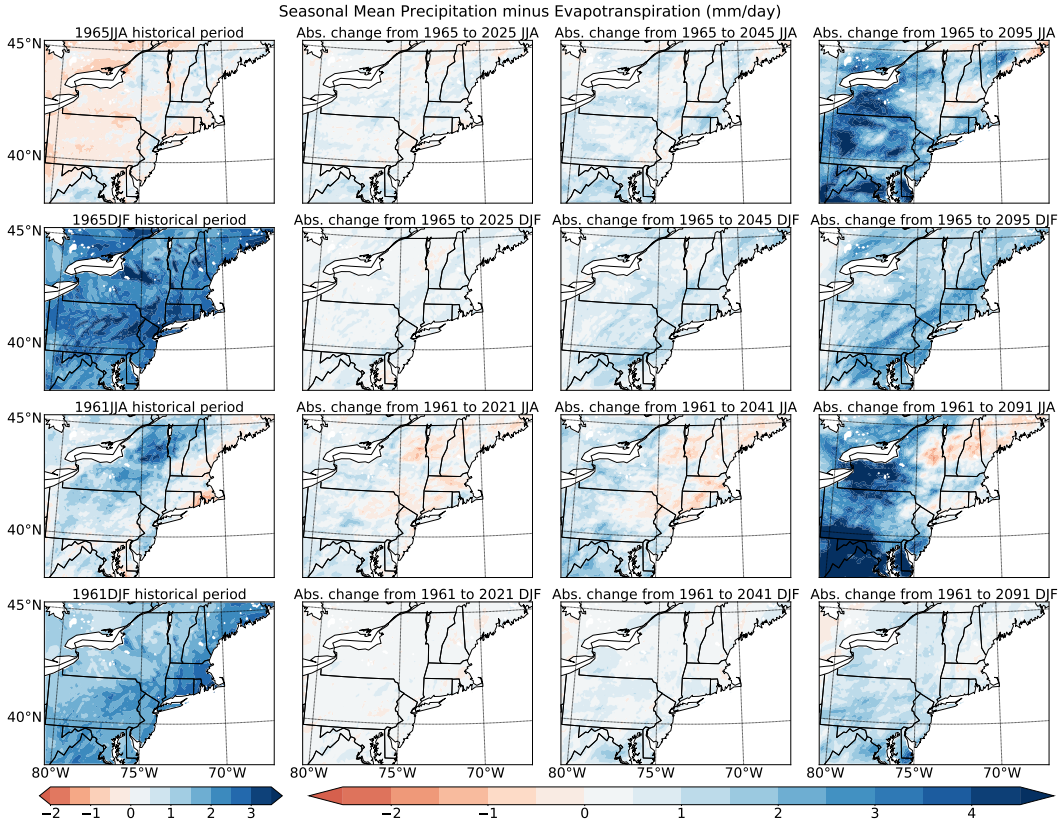

Figure 13. Seasonal mean net precipitation (mm/day) oover the 1965 dry exemplar and 1961 moderate exemplar,and projected changes in their future analogues for the JJA and DJF seasons.

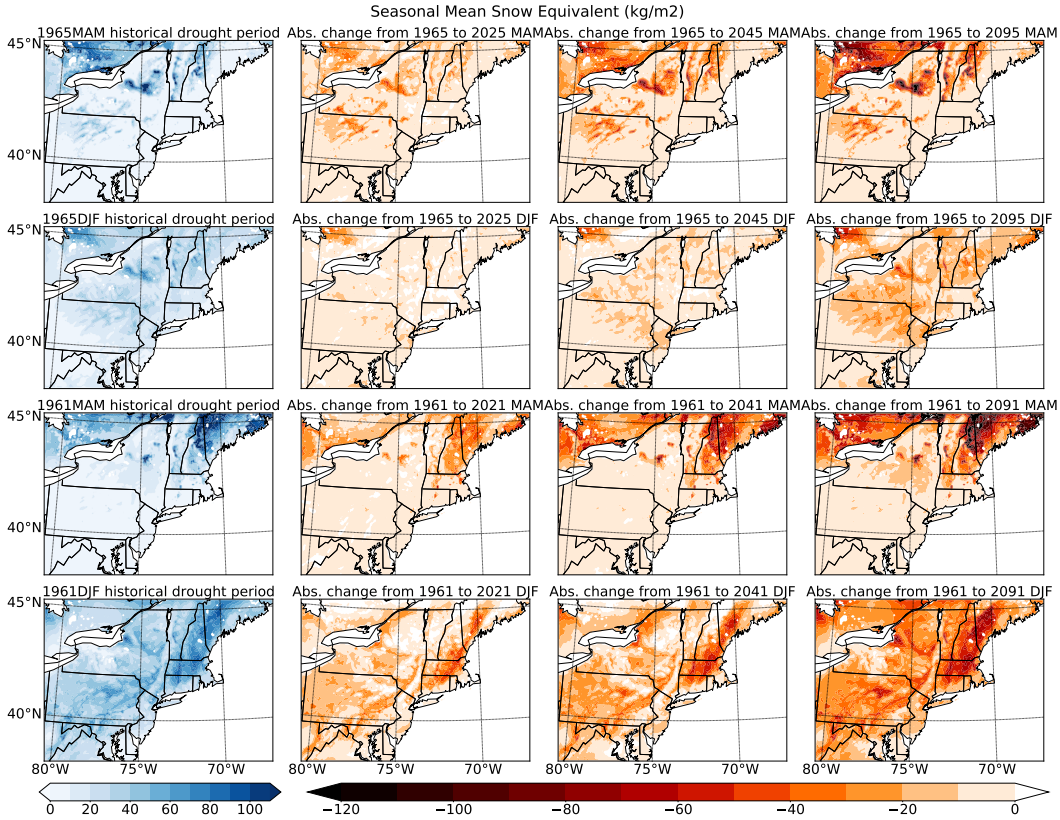

Figure 14. Seasonal mean snowpack absolute change (kg/m^2) over the 1965 dry exemplar and 1961 moderate exemplar,and projected changes in their future analogues for the JJA and DJF seasons.

a result of low precipitation. The depleted wintertime snowpack was a major reason for the seriousness of the drought in springtime; without snowmelt the surface runoff reached record lows. Over the northeastern corner of the domain the absolute change in SWE between 1965 and its future analogue is thus fairly small, because there is essentially no snow to remove (Figure 14). On the other hand, during the moderate periods this region has a healthy snowpack, which is severely depleted in the future (Figure 14).

4.7 Soil moisture and runoff

Soil moisture and runoff are two essential hydrologic variables and indicators of drought and water supply. In WRF-CLM4, soil moisture is accumulated over 10 layers; we focus on the average column soil moisture, which is the average soil moisture in each layer weighted by its thickness. Seasonal mean soil moisture over the 1965 and 1961 exemplar years (and differences in their future analogues) are depicted in Figure 16. Simulated runoff is directly output by WRF and its seasonal means and future change shown in Figure 17. Unsurprisingly, soil moisture trends upwards in accordance with net precipitation. Both dry and moderate periods have more soil moisture near the coast, however a significant increase can also be found during the moderate periods to the northeast. Although both net precipitation and soil moisture are generally increasing, surface runoff exhibits a decreasing trend in some regions, particularly during the dry periods, which we attribute to increasing snowmelt and frozen ground degradation and not obviously increased net precipitation (as discussed in section 4.5).

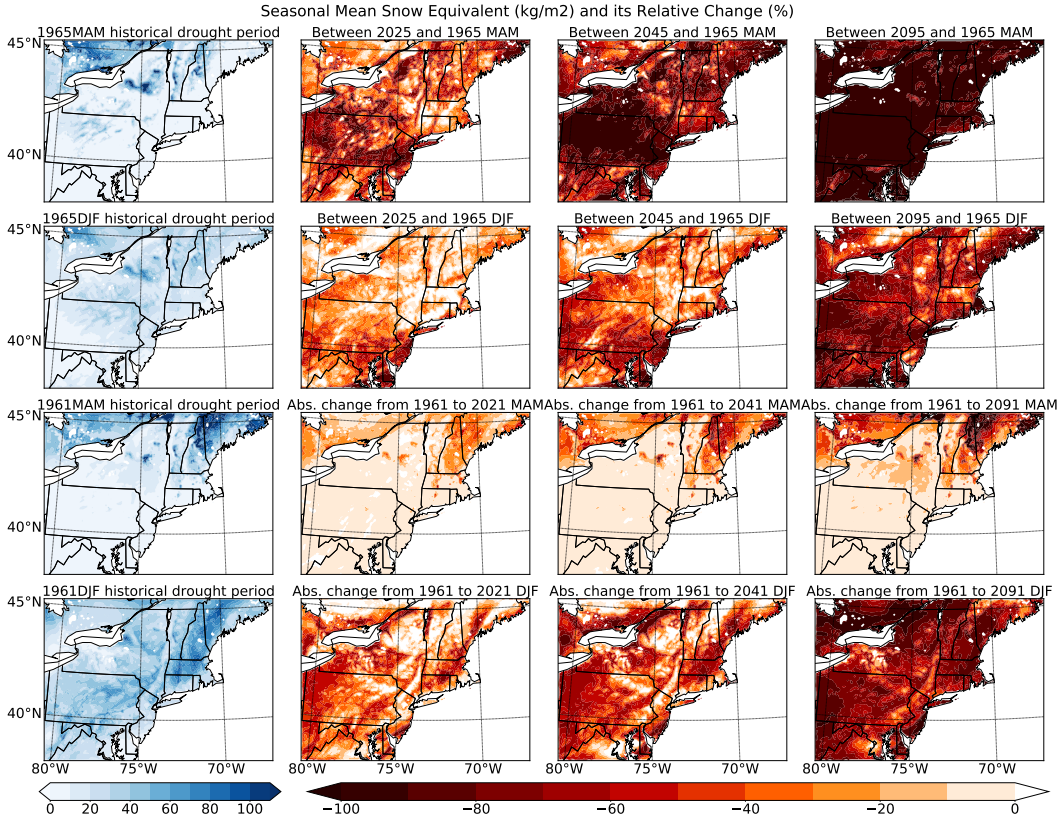

Figure 15. Seasonal mean snow water equivalent and its relative change over the 1965 dry exemplar and 1961 moderate exemplar,and projected changes in their future analogues for the JJA and DJF seasons.

4.7.1 Frozen ground degradation

Degradation of frozen ground is apparent for both the soil moisture and runoff fields regardless of time period. Frozen ground refers to permanently or seasonally frozen soil moisture, and can be assessed in terms of the number of freezing days (T. Zhang et al., 2003). Freezing of soil moisture drives up soil impermeability and reduces hydraulic conductivity, leading to a decline in soil infiltration and increase in surface runoff (more information on soil permeability in WRF-CLM4 is given in Appendix Appendix A). On the other hand, frozen ground degradation increases soil infiltration and reduces surface runoff. Frozen ground degradation is triggered by a loss of snowpack and reduction in freezing days, both of which are anticipated in a warmer climate. We argue that, particularly in DJF and MAM, frozen ground degradation is even more important for affecting soil moisture and runoff than net precipitation.

First, we observe that, compared with the dry years (Figures 14 and 13), moderate years experience a significant summertime net precipitation decrease and soil moisture increase simultaneously in the northeast (particularly in Canada). Certainly this would appear contradictory if net precipitation was the only driver of soil moisture change. However, the discrepancy can instead be explained by increases in snowmelt accompanied by frozen ground degradation, leading to greater infiltration to soil. Because historical snowpack was essentially zero in this region during the dry period, absolute decreases in snowpack and and their recharge to soil moisture are also low in the future periods (Figure 14). But during the moderate period, abundant historical snowpack was present over the same region (Figure 14), resulting in far more snowmelt in spring and summer, and greater soil recharge and surface runoff under a warming climate. This extra recharge from snowmelt also explains why, during the moderate period, the surface runoff decrease is much smaller than during the dry period (Figure 17). It also illustrates why over the northeast, dry periods have a greater net precipitation increase but lower soil moisture increase.

What's more, our hypothesis that frozen ground degradation has essential impacts on moistening of the soil is evinced with the fact that there exists a pretty strong negative correlation between regional mean soil moisture change and freezing days change (-0.88) that is even larger than its correlation with regional mean net precipitation change (0.79) during the winter season of dry periods over the inner domain. And in a multivariate linear regression model, freezing degree days and net precipitation change are together strong predictors of soil moisture delta ($R^2 > 0.85$).

4.7.2 Shifting runoff seasonality

In general, regions whose historical temperatures are just below 0°C are the most vulnerable to frozen ground degradation, as any enhancement in temperature would prevent freezing of soil moisture. As the soils of these regions then permit greater infiltration, they are also the regions in our simulations that experience the greatest decrease in surface runoff. As a result, frozen ground degradation leaves a clear seasonal signature in the runoff field: In Figure 17 it is apparent that the regions with the most surface runoff decrease do overlap with regions of historically seasonally frozen soil, at lower latitudes in DJF and higher latitudes during MAM.

The most obvious decrease in runoff under dry conditions occurs in our New England subregion, also the most populated subregion of our domain (Figure 17), and one with significant surface water demand . Loss of snowpack and frozen ground degradation here can be implicated in producing lower runoff and more infiltration, especially in the late winter and early spring. Examination of the long term monthly mean runoff change (Figure 18) confirms our claim that the largest runoff decrease is in early spring when SWE and frost days are most reduced into the future. Over the dry period, the inner domain produces the largest historical regional monthly mean runoff in March due

to abundant recharge from snowmelt; however, by end-of-century, March monthly mean runoff is reduced from 0.330 to 0.155 μm/day (more than a 50% loss). In fact, by end-of-century the surface regional runoff in the dry period peak moves from March to August in response to increasing summer precipitation. The springtime decrease in runoff is even more obvious within the New England subregion (Figure S7), where reductions in frozen days and snow water equivalent are more pronounced (Figure 15). Shifting of surface runoff away from spring has important consequences for agriculture – as discussed in section 2, the water shortage from the 1960s drought was at is most severe in the early spring due to agricultural demands.

4.8 Drought indices

From our earlier analysis, a generally warming climate with greater precipitation, evaporation and snowmelt are likely for a future analogue to the 1960s drought. However, overall wetter mean conditions doesn't necessarily imply that such a drought comes with fewer challenges. After all, the impacts of drought are complex and the product of multiple variables. Given wetter conditions are accompanied by increased temperatures and evapotranspiration, which in turn magnify the need for water, it's important to consider compound indices of drought as applied to historical and future conditions.

Standardized Precipitation Index (SPI) is a widely used family of drought indicators designed to capture the intensity of meteorological drought conditions (Hayes et al., 2002; Svoboda & Fuchs, 2016). Specifically, the metrics SPIn quantify the accumulated departure from the mean of n consecutive months' accumulated precipitation. Smaller values of n are relevant for short-term droughts and larger values for long-term droughts. However, a key limitation of the basic SPI metric is that it cannot account for evapotranspiration, preventing it from capturing moisture demand, and making it unsuitable for detecting flash droughts. Therefore, here we examine a modified version of SPI which instead uses net precipitation in place of actual precipitation (hereafter referred to as standardized net precipitation index, SNPI). We choose not to employ Standardized Precipitation Evapotranspiration Index (SPEI) (Vicente-Serrano et al., 2010) since WRF-CLM4 provides an accurate and internally-consistent version of evapotranspiration directly (Lawrence et al., 2011; Xu et al., 2020), whereas SPEI would require an empirical calculation of potential evapotranspiration (ET0). Past work has also illustrated that over sufficiently wet regions SNPI and SPEI are largely indistinguishable (Beguería et al., 2014; Joetzjer et al., 2012). Details on the calculation of SNPI are provided in Appendix **??**. Our interpretation of SNPI values is analogous to the interpretation of SPI given in Table 2 (Guttman, 1999).

To begin, trends of long-term drought conditions are examined using SNPI24. The 1960s drought is clearly visible in Figure 19 (top), and appears as the driest period in the past 100 years. The year 1965 exhibits the lowest annual mean SNPI24 value, in accord with the claim that 1965 was the driest of the past century. These results validate the use of SNPI and its effectiveness for identifying drought conditions. Looking to the future, although both precipitation and evapotranspiration increase substantially, annual mean regional SNPI24 at 2025 is only about -1, barely classifying as a drought. Under further warming, 2045 actually becomes anomalously wet – with SNPI24 in 2041 actually surpassing any historical value of SNPI24. At the end of this century (2090s), SNPI24 in every year is larger than 2, indicative that even under the same dynamical conditions of the 1960s, the climate will be unprecedented compared to historical. These results generally suggest that the threat from long-term meteorological drought over the next century will be greatly diminished.

Although the climatological shift towards wetter conditions will mitigate long-term drought, we can still ask if extreme drought conditions are similarly mitigated on shorter time scales? In fact, our simulations suggest the answer is "probably not." Specifically,

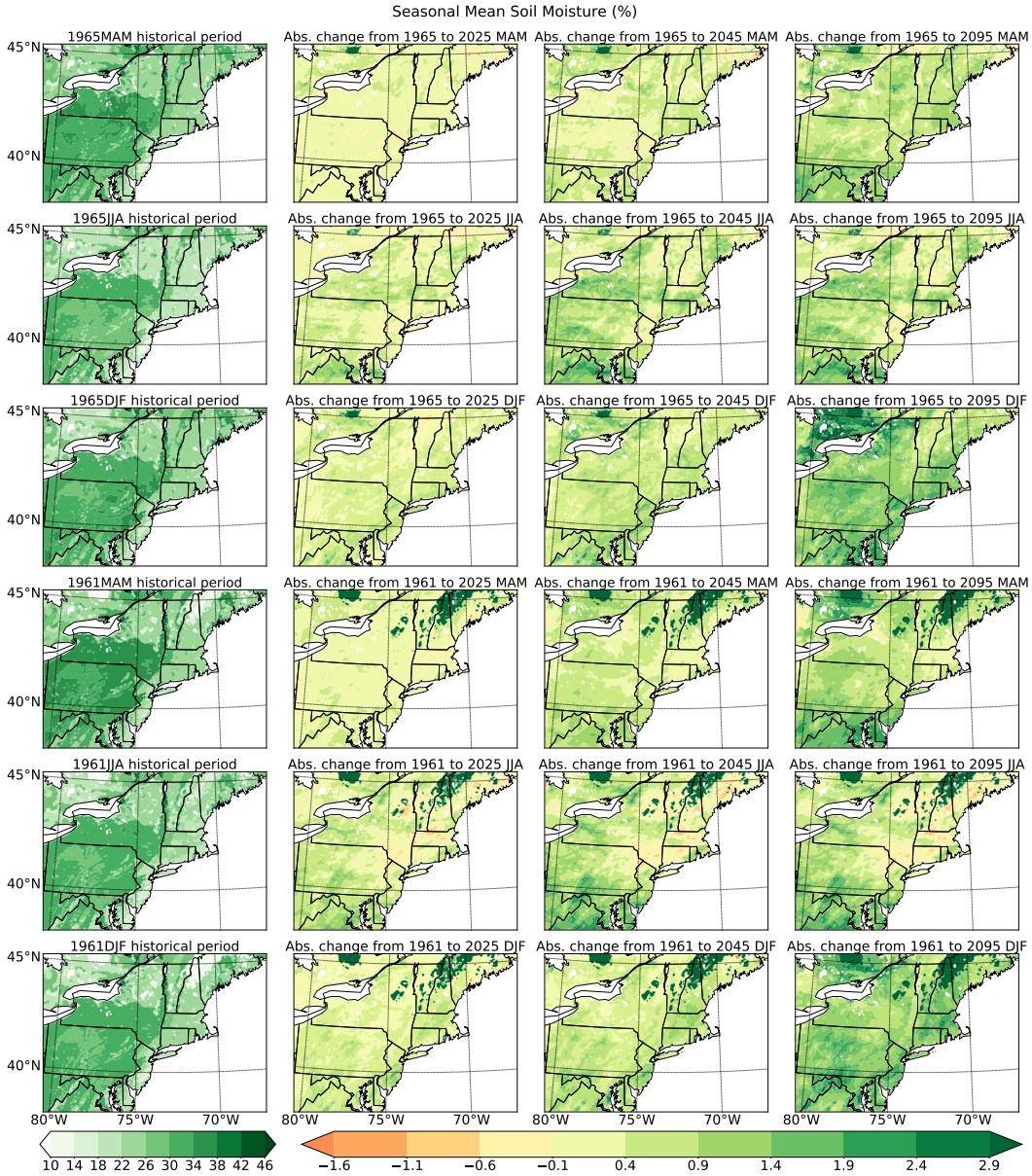

Figure 16. Seasonal mean soil moisture change (%) over the 1965 dry exemplar and 1961 moderate exemplar,and projected changes in their future analogues for the MAM, JJA, and DJF seasons.

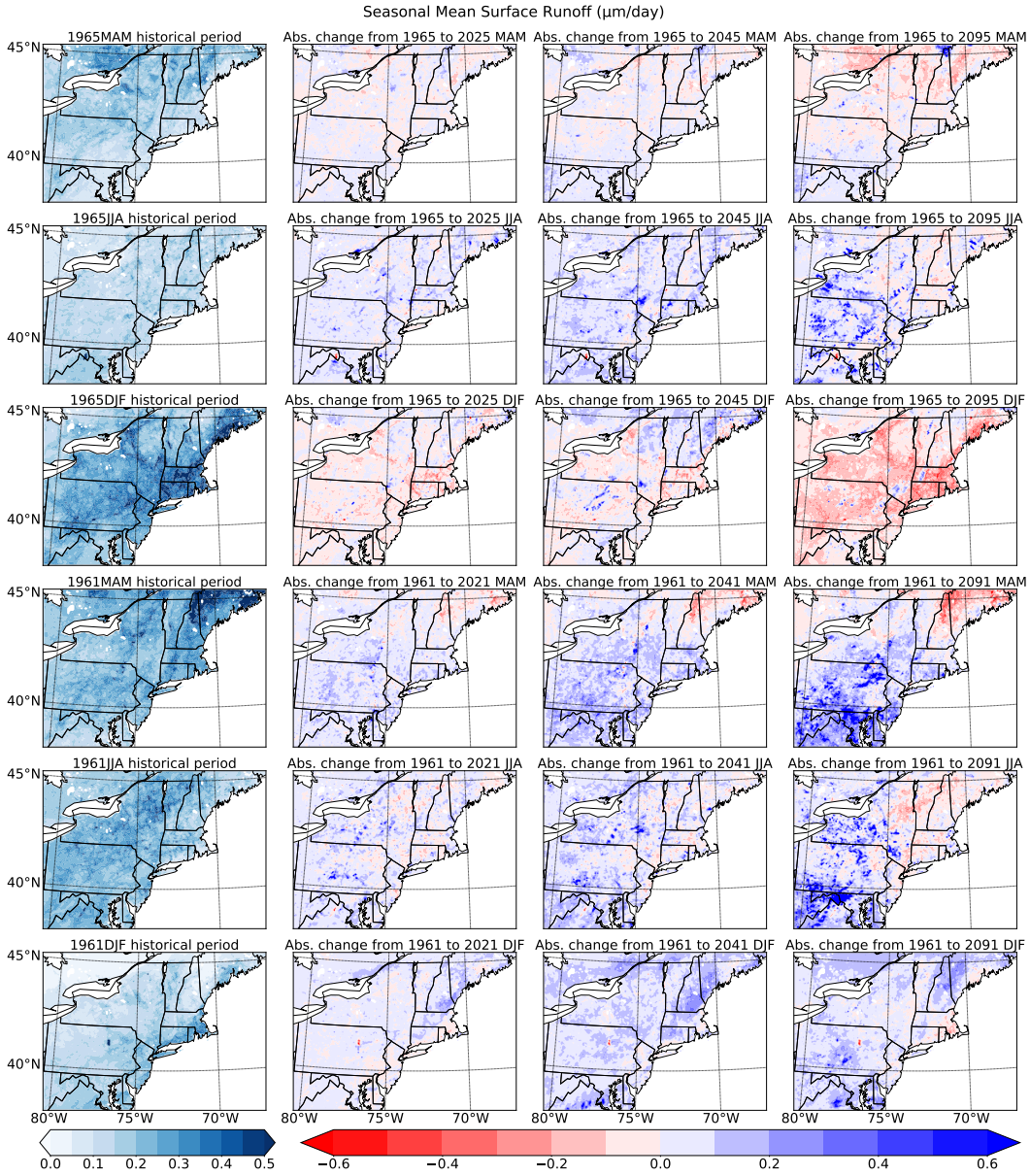

Figure 17. Seasonal mean runoff change (mm/day) over the 1965 dry year and 1961 moderate year, and projected changes in their future analogues for the MAM, JJA, and DJF seasons.

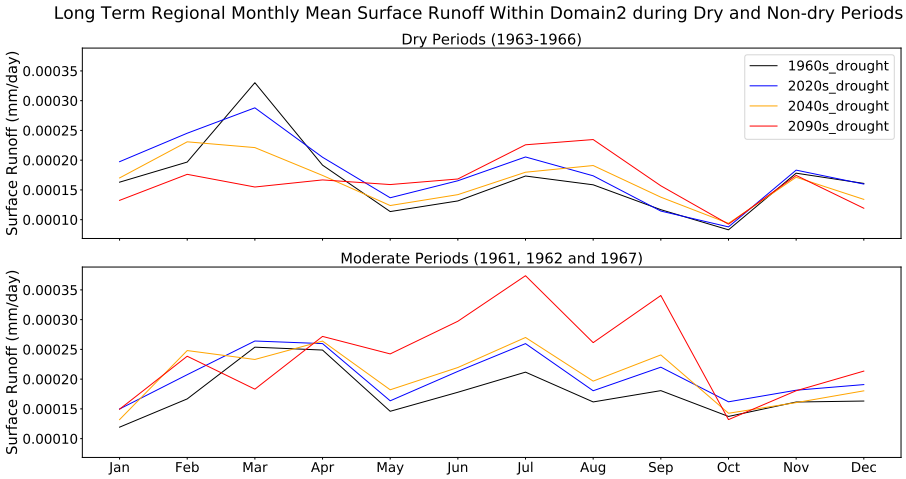

)

Figure 18. Regional long-term monthly mean runoff within the inner domain during dry years and moderate years.

Table 2. SNPI Classification following (Guttman, 1999).

SNPI Value	Conditions
SNPI $\geq$ 2	Extremely Wet
2 $>$ SNPI $\geq$ 1.5	Very Wet
1.5 $>$ SNPI $\geq$ 1	Moderately Wet
1 $>$ SNPI $>$ -1	Nearly Normal
-1.5 $<$ SNPI $\leq$ -1	Moderately Dry
-2 $<$ SNPI $\leq$ -1.5	Very Dry
SNPI $\leq$ -2	Extremely Dry

we calculate the SNPI1 of 1960s historical drought period (1963-1966) with that of the three future drought scenarios. Figure 19 (bottom) clearly shows that even as wetter months experience enhanced net precipitation, short-term extreme drought conditions persist. In fact, in the most extremely dry months (e.g. May 1964 and 1965), dryness is largely unchanged. Although the mean of SNPI1 during this period rises from -0.33 to 0.61, in accord with the general wetting trend, the standard deviation of SNPI1 also soars from 0.95 to 1.31, indicative of enhanced drought variability. This reflects enhanced climatological differences between dry and wet periods. More importantly, drought tends to happen more quickly – that is, a likely increase in the frequency *flash drought* (Christian et al., 2019). For example, April 2094 has a SNPI1 larger than 2 followed by a sudden drop to less than -3 in May; extremely dry conditions develop from extremely wet conditions in only one month! Suddenly adapting to dry conditions in such a short time would be an immense challenge for the region's water managers and stakeholders.

5 Conclusions

In this paper, the unprecedented 1960s NEUS drought is simulated as it occurred historically and subject to anticipated climate change from the early (2020-2027), middle (2040-2047) and late (2090-2097) 21^{st} century. To do so, the pseudo-global warming methodology is employed in WRF-CLM4: dynamical boundary conditions are iden-

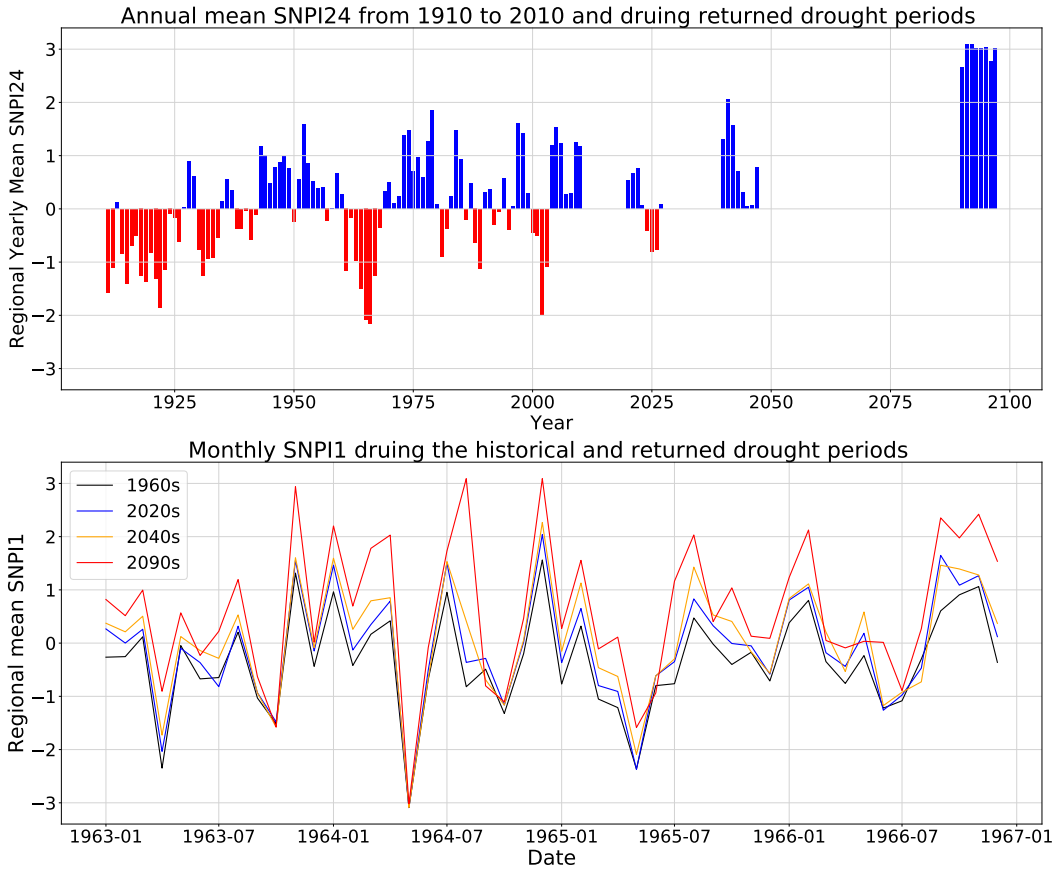

Figure 19. Regional annual mean SNPI24 and monthly mean SNPI1 within the New England subregion over historical and future periods.

tical to the historical period, while thermodynamics (atmospheric temperature, sea surface temperature and greenhouse gas concentration) are modified using the mean of four highly performant CMIP6 models under RCP8.5. Overall, our simulations reveal that although there is a significant wetting trend due to the overall increase in net precipitation (precipitation minus evapotranspiration) and moistening of the soil, this wetting is only apparent during non-dry months, while dry months with negative net precipitation are generally unchanged. This enhanced hydrologic variability has the potential to accelerate the development of drought, and make it possible for an extreme flash drought to rapidly emerge from wet conditions. Further, additional socioeconomic challenges will arise because of the surges in extreme hot days, unprecedented extreme heavy precipitation events, obvious shifts of climate patterns, and far less runoff in early spring as a result of frozen ground degradation and loss of snowpack. Our main findings are as follows:

First, as the prescribed lateral boundary conditions constrain temperatures, simulated years within each period have nearly the same regional mean warming. Compared with the 1960s period, the annual regional warming overland is 1.92-2.01°C in the 2020s, 3.16-3.27°C in the 2040s, and 6.74-6.87°C in the 2090s. However, significant spatial and temporal differences in warming emerge. For instance, cold regions warm faster than warm regions – a result that is more obvious at winter. Surging extreme heat days also make heat waves a potential problem over the NEUS in the future. Compared with more moderate periods, dry periods will experience a greater increase in both mean and extreme values of annual maximum daily temperature. Whereas each year of the historical period had less than 10 extreme heat days, the 2020s period had 7 - 30 extreme heat days, the 2040s had 14 - 40 days, and the 2090s had 52 - 79 days. Potential risks related to extreme hot weather include heatstroke and death.

Second, a clear annual mean precipitation increase emerges over the NEUS into the future (Figure 3). Regional annual mean precipitation increases by approximately 15%, 27% and 70% at the beginning, middle and end of the 21^{st} century. Precipitation increases more in regions with higher historical mean precipitation, especially in the winter in both dry and non-dry periods (with spatial correlation around 0.6). After accounting for increased evapotranspiration, most regions maintain a positive net precipitation change. A standardized drought index (SNPI24) is employed to show the gradual transformation from extremely dry to extremely wet conditions: Qualitatively, annual mean conditions in the 2020s are moderately dry, nearly neutral in the 2040s, and extremely wet in the 2090s. However, this does not imply extremely dry conditions at the monthly scale will vanish in the future: Because precipitation increase is only apparent in wet months, months with negative net precipitation are largely unchanged from historical. Consequently, our simulations suggest "wet months get wetter but dry months get drier (or are unchanged)." Consequently, net precipitation variability increases in a warming climate. Higher temperatures and enhanced evapotranspiration may produce flashier flash droughts and require longer lead times on water planning. Our simulations produce instances of extremely dry months (SNPI1 $\leq$ -2) that immediately follow extremely wet conditions (SNPI1 $\geq$ 2) in the 2090s. Such sudden drying could be devastating to agriculture, especially during the growing season. Drought monitoring systems working on shorter timescales that further incorporate short-term forecasting would be desirable in this case, though limitations on predictability could limit their value.

Third, increased precipitation amount and variability will drive more frequent and intense extreme storm events. Averaged over the simulation region, the probability of annual maximum precipitation exceeding 100 mm/day increases from 7.16% in the 1960s to 25.19% in the 2090s during dry periods, and from 6.28% at 1960s to 36.45% in the 2090s during moderate periods. The most extreme (99th percentile) regional mean precipitation intensifies by more than 58% and 51% by the end of this century during moderate and dry periods, respectively. Extreme precipitation brings with it a high risk of

flooding needed investments in protective infrastructure. Extreme precipitation from tropical cyclones wasn't touched on in this paper, although Hurricane Donna was captured in our simulation period; as in (Reed et al., 2020), we anticipate that climate change will increase precipitation, intensity, and size of these storms.

Fourth, significant warming in colder regions of the domain induces a substantial decrease in the number of regional mean freezing days and snowpack totals. We see a 60% decrease in the mean number of days with minimum daily temperature below 0°C, and a greater than 75% loss of snow water equivalent in the 2090s winter period versus historical. Consequently, we anticipate substantial degradation of frozen ground, which will increase soil infiltration and result in more water recharging to soil instead of surface runoff. More precipitation will occur as rainfall instead of snow, and snowmelt will happen earlier, essentially eliminating spring snowpack. Consequently surface runoff will decrease in spring due to lack of recharge from snowmelt.

Fifth, although it's intuitive that increases in net precipitation would produce more soil moisture and surface runoff, we argue that frozen ground degradation plays a larger role here. In support of this claim, summers of the moderate period feature a northeastern region with obviously reduced net precipitation, but the most significant increase in soil moisture. This directly opposes expectations if only net precipitation were implicated in moister soil. However, we find that reduced snowpack and freezing days permits greater infiltration from snow melting – in fact, during the winter season of dry periods, a strong negative correlation (-0.88) emerges between the change in the regional mean number of freezing days and soil moisture. This correlation is even larger than the positive correlation between the regional net precipitation change and soil moisture change.

Finally, we project a decrease in surface runoff during the winter and spring because of less snowmelt, along with increased infiltration to the soil due to the frozen ground degradation. Our simulations suggest March surface runoff decreases more than 50% in the 2090s dry periods compared with the 1960s drought period. This raises the specter of water shortages resulting from insufficient early spring runoff. From our simulations, we project the growing season to be the most vulnerable to anticipated future changes. In conjunction with increased water demand from higher temperatures, a reduction in available water poses great socioeconomic challenges.

This study primarily focuses on seasonal and regional scale changes, but ignores the consequences of particular weather events that occur on finer temporal and spatial scales. Given that the finest spatial and temporal resolution of our simulation is 9 km and 6 hours, our dataset could enable deeper exploration into specific events, along with their underlying process drivers. For example, this data could enable a better understanding of the strongest hurricane during 1960s period – Hurricane Donna – and its manifestation in the future in this region. Questions also remain about the potential for flash drought in this region under more general dynamical conditions, and how the 1960s drought compares to potentially more extreme droughts of the future for this region. Finally, given the simplifications made in CLM, there are substantial uncertainties in historical and projected surface and groundwater hydrology in these simulations; consequently it would be insightful to examine the response of a process-based hydrologic model to forcing data from these simulations.

Appendix A Soil degradation in WRF-CLM4

In the land model we used (WRF-CLM4), the soil infiltration factor is defined by equation A1. We can see that, when there is less freezing days, for each soil layer i, the ice contents ($w_{ice,i}$) will decrease and the liquid water contents ($w_{liq,i}$) will increase so that the impermeable fraction $f_{frz,i}$ will consequently decrease too which indicates that

the soil layers are less impermeable and there will be more infiltration to recharge the soil moisture (Oleson et al., 2010) .

$$f_{frz,i} = \frac{exp[-\alpha(1 - \frac{w_{ice,i}}{w_{ice,i}+w_{liq,i}})] - exp(-\alpha)}{1 - exp(-\alpha)} \tag{A1}$$

where $f_{frz,i}$ is the impermeable fraction which impacts the infiltration capacity, $w_{ice,i}$ and $w_{liq,i}$ ($kg \times m^{-2}$)are the ice and liquid water contents of soil layer i. $\alpha = 3$ is an adjustable scale-dependent parameter.

Appendix B Calculation of standardized net precipitation index (SNPI)

In this study SNPI is calculated analogous to SPI (Hayes et al., 2002; Svoboda & Fuchs, 2016), with a small modification for robustness. Generally, SPI is calculated by fitting the raw data to a gamma distribution, and then transforming it to be normally distributed. But under extremely dry conditions, evapotranspiration may exceed the precipitation giving a negative net precipitation, and so violate the requirements of the Gamma distribution. Thus we follow (Adams, 2017) and adjust the net precipitation data to make sure all data is non-negative prior to the fit:

$$\text{Net Precipitation}_{n,i} = \text{Net Precipitation}_{n,i} - \min(\text{Net Precipitation}) \tag{B1}$$

The calibration of SPI is sensitive to the quantity of data employed (following (Guttman, 1999) more than 50 years data is recommended). Since our WRF-CLM4 simulations are each only 8 years long, we instead combine the historical precipitation and evapotranspiration data from CERA20C R7 from 1910 to 2010 with our 1960s historical simulation to build a 101 years historical net precipitation time series data as the calibration period of SNPI for 3 future simulations (2020s, 2040s and 2090s). Namely, with the assumption that net precipitation nearly following the gamma distribution, all our data will be transformed to a normal distribution from a gamma distribution with the parameters calculated based on the historical data from 1910 to 2010. Our rationale for only using the historical period to calibrate the SNPI is to prevent our future drought projections from impacting the SNPI of the historical drought. To ensure our simulation data are consistent with CERA20C R7, WRF-CLM4 simulations are corrected by adding the regional mean differences between CERA20C R7 and WRF over the historical period (1961-1967).

Acknowledgments

We would like to thank Melissa Bukovsky, Rachel McCrary, and Zexuan Xu for their insights into proper execution of these regional simulations. We would also like to thank Shu-Hua Chen for granting us computer time to perform some of these simulations. This research was supported by the RGMA program area(s) in the U.S. Department of Energy's Office of Biological and Environmental Research as part of the multi-program, collaborative Integrated Coastal Modeling (ICoM) project. PAU was supported by Department of Energy Office of Science award number DE-SC0016605, "A Framework for Improving Analysis and Modeling of Earth System and Intersectoral Dynamics at Regional Scales (HyperFACETS)." This project is also supported by the National Institute of Food and Agriculture, U.S. Department of Agriculture, hatch project under California Agricultural Experiment Station project accession no. 1016611. We acknowledge the World Climate Research Programme, which, through its Working Group on Coupled Modelling, coordinated and promoted CMIP6. We thank the climate modeling groups for producing and making available their model output, the Earth System Grid Federation (ESGF) for archiving the data and providing access, and the multiple funding agencies who sup-

port CMIP6 and ESGF. The WRF model simulation data mentioned in this paper is available from ZENODO at https://doi.org/10.5281/zenodo.4310852.

References

Adams, J. (2017). *climate-indices, an open source python library providing reference implementations of commonly used climate indices.* `https://github.com/monocongo/climate_indices`.

Andreadis, K. M., & Lettenmaier, D. P. (2006). Trends in 20th century drought over the continental United States. *Geophysical Research Letters*, *33*(10).

Barksdale, H. C. (1968). *The northeast water supply crisis of the 1960's* (Tech. Rep.). Reston, VA: US Government Printing Office.

Barksdale, H. C., O'Bryan, D., & Schneider, W. J. (1966). *Effect of drought on water resources in the Northeast* (Tech. Rep.). Reston, VA: US Government Printing Office.

Beguería, S., Vicente-Serrano, S. M., Reig, F., & Latorre, B. (2014). Standardized precipitation evapotranspiration index (SPEI) revisited: parameter fitting, evapotranspiration models, tools, datasets and drought monitoring. *International Journal of Climatology*, *34*(10), 3001–3023.

Bretherton, C. S., & Park, S. (2009). A new moist turbulence parameterization in the Community Atmosphere Model. *Journal of Climate*, *22*(12), 3422–3448.

Burns, D. A., Klaus, J., & McHale, M. R. (2007). Recent climate trends and implications for water resources in the Catskill Mountain region, New York, USA. *Journal of Hydrology*, *336*(1-2), 155–170.

Byrne, M. P., & O'Gorman, P. A. (2015). The response of precipitation minus evapotranspiration to climate warming: Why the "wet-get-wetter, dry-get-drier" scaling does not hold over land. *Journal of Climate*, *28*(20), 8078–8092.

Case, J. L., Crosson, W. L., Kumar, S. V., Lapenta, W. M., & Peters-Lidard, C. D. (2008). Impacts of high-resolution land surface initialization on regional sensible weather forecasts from the WRF model. *Journal of Hydrometeorology*, *9*(6), 1249–1266.

Chou, C., & Neelin, J. D. (2004). Mechanisms of global warming impacts on regional tropical precipitation. *Journal of Climate*, *17*(13), 2688–2701.

Christian, J. I., Basara, J. B., Otkin, J. A., Hunt, E. D., Wakefield, R. A., Flanagan, P. X., & Xiao, X. (2019). A methodology for flash drought identification: Application of flash drought frequency across the United States. *Journal of Hydrometeorology*, *20*(5), 833–846.

Cook, E. R., & Jacoby, G. C. (1977). Tree-ring-drought relationships in the Hudson Valley, New York. *Science*, *198*(4315), 399–401.

Dai, A., Trenberth, K. E., & Qian, T. (2004). A global dataset of Palmer Drought Severity Index for 1870–2002: Relationship with soil moisture and effects of surface warming. *Journal of Hydrometeorology*, *5*(6), 1117–1130.

DeGaetano, A. T. (1999). A temporal comparison of drought impacts and responses in the New York city metropolitan area. *Climatic Change*, *42*(3), 539–560.

Demaria, E. M., Palmer, R. N., & Roundy, J. K. (2016). Regional climate change projections of streamflow characteristics in the Northeast and Midwest US. *Journal of Hydrology: Regional Studies*, *5*, 309–323.

Donat, M. G., Lowry, A. L., Alexander, L. V., O'Gorman, P. A., & Maher, N. (2016). More extreme precipitation in the world's dry and wet regions. *Nature Climate Change*, *6*(5), 508–513.

European Centre for Medium-Range Weather Forecasts. (2016). *Coupled ECMWF Re-Analysis system of the 20th-century.* `https://www.ecmwf.int/en/forecasts/datasets/reanalysis-datasets/cera-20c`.

Frumhoff, P. C., McCarthy, J. J., Melillo, J. M., Moser, S. C., & Wuebbles, D. J. e. a. (2007). Confronting climate change in the US Northeast: Sci-

ence, impacts, and solutions. *Confronting climate change in the US Northeast: science, impacts, and solutions.*.

Ganetis, S. A., & Colle, B. A. (2015). The thermodynamic and microphysical evolution of an intense snowband during the northeast US blizzard of 8–9 February 2013. *Monthly Weather Review*, *143*(10), 4104–4125.

Guttman, N. B. (1999). Accepting the standardized precipitation index: a calculation algorithm 1. *JAWRA Journal of the American Water Resources Association*, *35*(2), 311–322.

Hayes, M. J., Alvord, C., & Lowrey, J. (2002). *Drought indices.* National Drought Mitigation Center, University of Nebraska.

Hayhoe, K., Wake, C., Anderson, B., Liang, X.-Z., Maurer, E., Zhu, J., ... Wuebbles, D. (2008). Regional climate change projections for the Northeast USA. *Mitigation and Adaptation Strategies for Global Change*, *13*(5-6), 425–436.

Hayhoe, K., Wake, C. P., Huntington, T. G., Luo, L., Schwartz, M. D., Sheffield, J., ... DeGaetano, A. e. a. (2007). Past and future changes in climate and hydrological indicators in the US Northeast. *Climate Dynamics*, *28*(4), 381–407.

Hobbs, J. J. (2008). *World regional geography.* Nelson Education.

Hoegh-Guldberg, O., Jacob, D., Bindi, M., Brown, S., Camilloni, I., Diedhiou, A., ... Guiot, J. e. a. (2018). Impacts of 1.5 °C global warming on natural and human systems. *Global warming of 1.5° C. An IPCC Special Report*.

Huntington, T. G., Hodgkins, G. A., Keim, B. D., & Dudley, R. W. (2004). Changes in the proportion of precipitation occurring as snow in New England (1949–2000). *Journal of Climate*, *17*(13), 2626–2636.

Iacono, M. J., Delamere, J. S., Mlawer, E. J., Shephard, M. W., Clough, S. A., & Collins, W. D. (2008). Radiative forcing by long-lived greenhouse gases: Calculations with the AER radiative transfer models. *Journal of Geophysical Research: Atmospheres*, *113*(D13).

Janes, B. E., & Brumbach, J. J. (1965). The 1964 Agriculture Drought in Connecticut. *University of Connecticut*.

Jiménez, P. A., Dudhia, J., González-Rouco, J. F., Navarro, J., Montávez, J. P., & García-Bustamante, E. (2012). A revised scheme for the WRF surface layer formulation. *Monthly Weather Review*, *140*(3), 898–918.

Jin, J., Miller, N. L., & Schlegel, N. (2010). Sensitivity study of four land surface schemes in the WRF model. *Advances in Meteorology*, *2010*.

Joetzjer, E., Douville, H., Delire, C., Ciais, P., Decharme, B., & Tyteca, S. (2012). Evaluation of drought indices at interannual to climate change timescales: a case study over the Amazon and Mississippi river basins. *Hydrology & Earth System Sciences Discussions*, *9*(11).

Kharin, V. V., Zwiers, F. W., Zhang, X., & Hegerl, G. C. (2007). Changes in temperature and precipitation extremes in the IPCC ensemble of global coupled model simulations. *Journal of Climate*, *20*(8), 1419–1444.

Kimura, F., Kitoh, A., Sumi, A., Asanuma, J., & Yatagai, A. (2007). Downscaling of the global warming projections to Turkey. *The Final Report of ICCAP*, *10*.

Krakauer, N. Y., Lakhankar, T., & Hudson, D. (2019). Trends in Drought over the Northeast United States. *Water*, *11*(9), 1834.

Lawrence, D. M., Oleson, K. W., Flanner, M. G., Thornton, P. E., Swenson, S. C., Lawrence, P. J., ... others (2011). Parameterization improvements and functional and structural advances in version 4 of the Community Land Model. *Journal of Advances in Modeling Earth Systems*, *3*(1).

Lindsey, R., & Dahlman, L. (2020). *Climate Change: Global Temperature.* National Oceanic and Atmospheric Administration.

Lyon, B., Christie-Blick, N., & Gluzberg, Y. (2005). Water Shortages, Development, and Drought in Rockland County, New York. *JAWRA Journal of the American Water Resources Association*, *41*(6), 1457–1469.

Melillo, J. M., Richmond, T., & Yohe, G. e. a. (2014). Climate change impacts in the United States. *Third National Climate Assessment*, *52*.

Moser, S. C., Kasperson, R. E., Yohe, G., & Agyeman, J. (2008). Adaptation to climate change in the Northeast United States: opportunities, processes, constraints. *Mitigation and Adaptation Strategies for Global Change*, *13*(5-6), 643–659.

Namias, J. (1966). Nature and possible causes of the northeastern United States drought during 1962–65. *Mon. Wea. Rev*, *94*(9), 543–554.

Neale, R. B., Chen, C.-C., Gettelman, A., Lauritzen, P. H., Park, S., Williamson, D. L., ... Lamarque, J.-F. e. a. (2010). Description of the NCAR community atmosphere model (CAM 5.0). *NCAR Tech. Note*, *1*(1), 1–12.

NOAA. (2020). *Heat Index definition by NOAA.* `https://www.weather.gov/safety/heat-index`.

of Economic Analysis, U. B. (2016). Gross domestic product (GDP) by state (millions of current dollars). *US Bureau of Economic Analysis*.

Oleson, K. W., Lawrence, D. M., Gordon, B., Flanner, M. G., Kluzek, E., Peter, J., ... others (2010). *Technical description of version 4.0 of the Community Land Model (CLM).* Citeseer.

Pfahl, S., O'Gorman, P. A., & Fischer, E. M. (2017). Understanding the regional pattern of projected future changes in extreme precipitation. *Nature Climate Change*, *7*(6), 423–427.

Powers, J. G., Klemp, J. B., Skamarock, W. C., Davis, C. A., Dudhia, J., Gill, D. O., ... Peckham, S. E. e. a. (2017). The weather research and forecasting model: Overview, system efforts, and future directions. *Bulletin of the American Meteorological Society*, *98*(8), 1717–1737.

Reed, K. A., Stansfield, A., Wehner, M., & Zarzycki, C. (2020). Forecasted attribution of the human influence on hurricane florence. *Science Advances*, *6*(1), eaaw9253.

Rothfusz, L. P., & Headquarters, N. S. R. (1990). The heat index equation (or, more than you ever wanted to know about heat index). *Fort Worth, Texas: National Oceanic and Atmospheric Administration, National Weather Service, Office of Meteorology*, *9023*.

Seager, R., Naik, N., & Vecchi, G. A. (2010). Thermodynamic and dynamic mechanisms for large-scale changes in the hydrological cycle in response to global warming. *Journal of Climate*, *23*(17), 4651–4668.

Seager, R., Pederson, N., Kushnir, Y., Nakamura, J., & Jurburg, S. (2012). The 1960s drought and the subsequent shift to a wetter climate in the Catskill Mountains region of the New York City watershed. *Journal of Climate*, *25*(19), 6721–6742.

Skamarock, W. C., Klemp, J. B., Dudhia, J., Gill, D. O., Barker, D. M., Wang, W., & Powers, J. G. (2008). 2005: A description of the advanced research WRF version 2. In *NCAR Tech. Note*.

Srivastava, A., Grotjahn, R., & Ullrich, P. (2020). Evaluation of historical CMIP6 model simulations of extreme precipitation over contiguous US regions. *Weather and Climate Extremes*, 100268.

Strzepek, K., Yohe, G., Neumann, J., & Boehlert, B. (2010). Characterizing changes in drought risk for the United States from climate change. *Environmental Research Letters*, *5*(4), 044012.

Svoboda, M., & Fuchs, B. (2016). Handbook of drought indicators and indices. Integrated drought management programme (IDMP), integrated drought management tools and guidelines series 2. *World Meteorological Organization and Global Water Partnership, Geneva, Switzerland*, *52*.

Ullrich, P., Xu, Z., Rhoades, A., Dettinger, M., Mount, J., Jones, A., & Vahmani, P. (2018). California's drought of the future: A midcentury recreation of the exceptional conditions of 2012–2017. *Earth's Future*, *6*(11), 1568–1587.

Van den Dool, H., Huang, J., & Fan, Y. (2003). Performance and analysis of the constructed analogue method applied to US soil moisture over 1981–2001. *Journal of Geophysical Research: Atmospheres*, *108*(D16).

Vicente-Serrano, S. M., Beguería, S., & López-Moreno, J. I. (2010). A multiscalar drought index sensitive to global warming: the standardized precipitation evapotranspiration index. *Journal of Climate*, *23*(7), 1696–1718.

Xu, X., Li, X., Wang, X., He, C., Tian, W., Tian, J., & Yang, L. (2020). Estimating daily evapotranspiration in the agricultural-pastoral ecotone in Northwest China: A comparative analysis of the Complementary Relationship, WRF-CLM4. 0, and WRF-Noah methods. *Science of The Total Environment*, 138635.

Zhang, G. J., & McFarlane, N. A. (1995). Role of convective scale momentum transport in climate simulation. *Journal of Geophysical Research: Atmospheres*, *100*(D1), 1417–1426.

Zhang, T., Barry, R., Knowles, K., Ling, F., & Armstrong, R. (2003). Distribution of seasonally and perennially frozen ground in the Northern Hemisphere. In *Proceedings of the 8th International Conference on Permafrost* (Vol. 2, pp. 1289–1294).